Functional separation of two distinct voltage gated calcium channels at the presynaptic terminal of *Drosophila* larval crawling motoneurons

Dissertation zur Erlangung des Grades Doktor der Naturwissenschaft

Am Fachbereich Biologie

Der Johannes Gutenberg-Universität Mainz

Institut für Entwicklungsbiologie und Neurobiologie

Niklas Krick

Geb. am 14.08.1992 in Mainz

Mainz, 2020

Dekan:

Erstgutachter:

Zweitgutachter:

Tag der mündlichen Prüfung:

Table of content

Throughout the text, the L-Type Voltage gated calcium channel will be referred to as Dmca1D, while in Figures it is referred to as Ca_v1.

Summary

At the presynaptic terminal of chemical synapses, release probability of synaptic vesicles must be tightly controlled, while at the same time vesicle recycling and changes in release probability need to occur side by side and must be dynamically adapted to a changing external input and internal state. These three mechanisms are heavily calcium dependent thus needing different calcium nano- and/or microdomains with specific spatio-temporal identities. Calcium nano- and/or microdomains are produced by clusters of voltage gated calcium channels (VGCC), and the characteristics depend on the abundance and individual gating properties of the respective calcium channels and on the calcium buffering properties of soluble buffers, calcium binding proteins and extrusion pumps. Hence, the major questions of this thesis are, what is the underlying mechanism that enables separate regulation of these crucial, calcium dependent presynaptic mechanisms and what are its molecular components. Combining *Drosophila* genetics, electrophysiology and imaging techniques, I uncover a new mechanism that allows simultaneous calcium signaling for exo and endocytosis in the limited space of presynaptic terminals.

In *Drosophila* three genes for VGCCs exist, Dmca1D, a homolog of vertebrate Ca_v1 channels, Dmca1A, the Ca_v2 homolog and DmαG as a homolog for vertebrate Ca_v3 channels. It has long been known that action potential triggered SV exocytosis is mediated by calcium influx through the Dmca1A calcium channel that localizes in the active zone, in close proximity to the readily releasable vesicle pool. In this thesis, I now discovered that action potential mediated calcium signaling for short term plasticity, as well as activity dependent endocytosis regulation, are mediated via the Dmca1D calcium channel, localized outside the active zone. Even though exo- and endocytosis need to occur on different timescales and rely on different calcium concentrations, I demonstrate that despite the physical distance between both calcium sources, the active zone calcium nanodomain for exocytosis is actively protected from peri-active zone calcium signaling by the plasma membrane bound calcium ATPase PMCA.

This newly identified mechanism of separate yet parallel calcium signaling significantly increases the understanding of presynaptic calcium handling during activity and gives rise to conceptually new functions of peri-active zone molecules and their effects on stable presynaptic function and plasticity.

1. Introduction

1.1 Intracellular Calcium Signaling

Calcium entry into a cell and the associated downstream signaling pathways are the foundation of many fundamental processes in all living cells (Islam, 2020). Calcium can regulate the expression of genes (Hardingham et al., 1998), induces secretion of hormones (Brown et al., 1985), is responsible for muscle contractions (Heilbrunn and Wiercinski, 1947), synaptic vesicle release (Katz and Miledi, 1966) and the induction of synaptic plasticity (Klein et al., 1980). These processes are orchestrated by countless different cell structures, channels, receptors, pumps and many more which often work in coorporation to either generate or decode calcium signals (Islam, 2020). These processes are studied in many different model and theoretical systems to understand the processes of life from normal physiological mechanisms to aging and disease.

In neuroscience, calcium signaling and its downstream mechanisms, have been under investigation for almost six decades (Dolphin, 2018). Even though, already in 1883, Ringer showed the necessity of calcium for heart muscle contraction (Ringer, 1883), neuroscience research mainly focused on sodium and potassium and their contribution to the generation of action potentials. It was not until the 1950s, when Fatt, Katz and Ginsborg observed that calcium generates action potential like spikes in the crustacean muscle (Fatt and Ginsborg, 1958; Fatt and Katz, 1952) and finally in 1967, when Katz and Miledi showed that calcium is essential for neurotransmitter release (Katz and Miledi, 1966). It was indisputable, that calcium signaling and its entry routes provide key insight into the physiological functions of neurons. One way calcium can pass the neuronal cell membrane is through voltage gated calcium channels (VGCC). This has manifold functions in the dendrites, soma, axon and axon terminals of every neuron. Especially at the excitable neuronal membrane, calcium provides two functions. First it functions as a charge carrier and therefore can be used in dendrites to amplify synaptic input (Heckman et al., 2003) or in axons to enhance action potential firing (Kadas et al., 2017; Ramírez-Latorre, 2012). Second it functions as a second messenger in regulating gene transcription (Hutchinson et al., 2015), the regulation of enzymatic processes (Dolmetsch et al., 2001), or, as already described, action potential triggered synaptic vesicle release at presynaptic terminals. Calcium as a second messenger is highly efficient because of the extremely low intracellular calcium

concentration which is maintained at rest between 10-100nM by efficient buffer uptake, and extrusion mechanisms (Berridge et al., 2000; Dolphin, 2016).Therefore, calcium signals are precisely controlled in time and space, and strongly affected by both, the position of calcium channels and their respective calcium gating kinetics.

The focus of this study is the function of VGCCs at presynaptic terminals. Synaptic vesicle release at chemical synapses is probably the best described coupling of activity induced, intracellular calcium signaling mediated by VGCCs (Berridge et al., 2000; Gerber and Sudhof, 2002; Gerber et al., 2001; Katz and Miledi, 1966; Khvotchev et al., 2000; Luo and Südhof, 2017; Sclip et al., 2018; Südhof, 2004; Sugita and Südhof, 2000; Voets et al., 2001; Wang et al., 2019; Zhang et al., 1994). Upon action potential invasion into the presynaptic terminal, calcium enters the cell through VGCC, binds to the synaptic vesicle (SV) protein synaptotagmin and induces SV release. At most synapses, this type of synaptic vesicle release is mediated via Ca_V2 channels localized at the active zones. Specialized synapses, like the so-called ribbon synapses, mostly rely on Ca_V1 channels for synaptic vesicle release.

We show that, besides the Ca_V2 homolog Dmca1A, the Ca_V1 homolog Dmca1D is present at presynaptic terminals of *Drosophila* larval crawling motoneurons and analyzed its contribution and function in presynaptic calcium signaling. Additionally, we revealed the precise location of the previously described plasma membrane bound calcium ATPase (PMCA) within presynaptic nerve terminals. The main focus of this thesis was to analyze the interplay of the two presynaptically localized VGCCs with the PMCA in the context of presynaptic calcium signaling and the associated effects for SV release, recycling, short term plasticity, and the dynamic properties of synaptic transmission.

1.2 Voltage gated calcium channels

The excitable membrane of neurons is equipped with a multitude of voltage dependent ion channels such as calcium permeable channels. At resting membrane potentials between -60 to -80mV, VGCCs remain closed and open upon membrane depolarization. A distinction is made between high voltage activated (HVA) and low voltage activated (LVA) calcium channels. HVA calcium channels open at around -30mV, whereas LVA channels open at around -50mV. Nevertheless, the basic topology of all voltage gated calcium channels is similar (Fig. 1). They consist of

different subunits, the α_1 subunit, $\alpha_2\delta$, β and in muscles the γ subunit, each of which fulfills a specific function.

The α_1 subunit is the pore forming subunit and gives rise to the basic physiological and pharmacological properties of a calcium channel. It is composed of homologous repeats each containing six transmembrane segments, S1-S6, that are arranged clockwise. The voltage sensing domain (VSD) is made from S1-4 while the positively charged S4 domain contains the actual voltage sensor (Wu et al., 2016; Zhao et al., 2019), and S5&6 are connected via an extracellular P-loop containing an acidic residue forming a windowed dome above the selectivity filter (Wu et al., 2016). In vertebrates the different α_1 subunits are encoded by 10 different CACNA genes (Catterall et al., 2003), and their resulting proteins are being separated in three major classes, Ca_v1-3. The Ca_v1 channels ($Ca_v1.1$- $Ca_v1.4$) are read from four different genes and are also known as L-Type calcium channels, are high voltage activated, and provide a long lasting, sustained calcium inward current. They are typically sensitive to dihydropyridines and have a manifold of functions in many different tissues. For example $Ca_v1.1$ channels are needed for muscle contraction in skeletal muscles, $Ca_v1.2$ channels augment smooth muscle tone but are also needed for insulin secretion in the pancreas, the heart action potential as well as long term potentiation in the Schaffer collateral neurons of the hippocampus (Moosmang et al., 2005; Zamponi et al., 2015). $Ca_v1.3$ channels are reported in auditory hair cells, mediating neurotransmitter release, provide pacemaking in the sinoatrial node of the heart, or contribute to adrenaline secretion of chromaffin cells in the adrenal medulla (Zamponi et al., 2015). The $Ca_v1.4$ channels are found in the retina where they contribute to neurotransmitter release from photoreceptors and bipolar cells (Zamponi et al., 2015). This is only a small subset of the diverse functions of Ca_v1 channels. In *Drosophila* the four different genes for Ca_v1 channels have only one homolog which encodes for the Dmca1D channel (see 1.3).

The Ca_v2 channel family ($Ca_v2.1$- $Ca_v2.3$) includes three different genes for voltage gated calcium channels which are also called P/Q-, N- and R-Type (Catterall, 2011). Their best-described function is the coupling between action potential invasion and synaptic vesicle release, which is conserved from invertebrates to vertebrates (Catterall, 2011). This is also true for the *Drosophila* homolog, Dmca1A or cacophony, which is the only Drosophila Ca_v2 channel homolog. In addition to its fundamental function in synaptic vesicle release, which is also discussed later in this theses,

Dmca1A is found in the soma and the dendrites of the adult flight motoneuron MN5, mediating 90% of the somatodendritic calcium current (Ryglewski et al., 2012). Furthermore the Dmca1A channels is capable of mediating HVA as well as LVA currents (Ryglewski et al., 2012) which is caused by mutually exclusive and alternative splicing (personal communication).

Three genes encode for Ca_v3 α_1 subunits ($Ca_v3.1$- $Ca_v3.3$). Ca_v3 channels are low threshold (Tang et al., 1988) activated and meditate a short, transient current, also referred to as T-Type current. Ca_v3 channel have a small single channel conductance (8pS), compared to Ca_v1 (25pS) and Ca_v2 (13pS) (Hille, 2001). Due to their low voltage activity, they have important functions in the regulation of neuronal excitability in thalamocortical circuits and the cerebellum, contribute to pacemaker activity in the sinoatrial node and the thalamus, in rebound bursting in thalamocortical neurons (Simms and Zamponi, 2014) as well as evoked hormone secretion (Zamponi et al., 2015). Additionally they have been linked to synaptic vesicle release from presynaptic afferent nerve terminals in the dorsal horn (Jacus et al., 2012). The *Drosophila* homolog for $Ca_v3.1$- $Ca_v3.3$ is encoded by the gene DmαG (Littleton and Ganetzky, 2000). In the adult flight motoneuron MN5, DmαG mediates 35% of the low voltage activated T-Type current measured from the soma, activates between -70 to -60 mV and can be selectively blocked by the T-Type channel blocker amiloride (Ryglewski et al., 2012).

To be fully functional, Ca_v1 and Ca_v2 α_1 subunits interact with the auxiliary subunits $\alpha_2\delta$, β, and in muscles, the γ subunit, while Ca_v3 can function without binding any further subunit (Dolphin, 2016; Zamponi et al., 2015). The extracellular $\alpha_2\delta$ subunit has reported functions in HVA calcium channel trafficking as well as surfacing and affects the biophysical properties of HVA calcium channels (Dolphin, 2016; Heinrich and Ryglewski, 2019). In vertebrates, four different genes for $\alpha_2\delta$ subunits exist ($\alpha_2\delta$1-4) and their mis-regulation has been associated with neurological diseases such as neuropathic pain ($\alpha_2\delta$-1), epilepsy ($\alpha_2\delta$-1), night blindness ($\alpha_2\delta$-4), autism ($\alpha_2\delta$-3) and many more (Dolphin, 2016). *Drosophila* also expresses four genes for $\alpha_2\delta$ subunits which are also named $\alpha_2\delta$1-4, while $\alpha_2\delta$-3 is also called straightjacket (stj) (Heinrich and Ryglewski, 2019). A recent study from our lab (Heinrich and Ryglewski, 2019), specifically targeted the functions of $\alpha_2\delta$-1 and $\alpha_2\delta$-3 in larval and adult motoneurons. Contrasting to the findings from heterologous expression systems, where any $\alpha_2\delta$ subunit can mediate sufficient α_1 channel function, they showed that $\alpha_2\delta$-1 specifically

functions in VGCC allocation to dendrites and the axon and a knockdown of $\alpha_2\delta$-1 results in decreased total dendritic length and increased calcium influx into the axon. $\alpha_2\delta$-3 on the other hand is necessary for normal synaptic transmission as well as somatodendritic and axonal Ca_v1 and Ca_v2 current amplitudes. Knockdown of $\alpha_2\delta$-3 causes reduced synaptic transmission, as well as reduced somatodendritic calcium current amplitude and reduced calcium influx into the axon. These specific functions in of $\alpha_2\delta$-1 and $\alpha_2\delta$-3 in different subcellular compartments for correct Ca_v1 and Ca_v2 function further underline the manifold of functions resulting from different α_1/ $\alpha_2\delta$ combinations.

Besides the $\alpha_2\delta$ subunit, the β subunit is inevitable for full calcium channel function. It is encoded by four genes in vertebrates (β_1- β_4) (Dolphin, 2016) and one gene in invertebrates and is bound intracellularly to α_1 subunit. The β subunit promotes the right folding of calcium channels and influences calcium dependent inactivation (Dolphin, 2016). In *Drosophila* the β subunit is necessary for correct VGCC activity and therefore synaptic transmission and development of the neuromuscular junction (Gaudet et al., 2011) as well as correct dendritic pruning in sensory neurons (Kanamori et al., 2013).

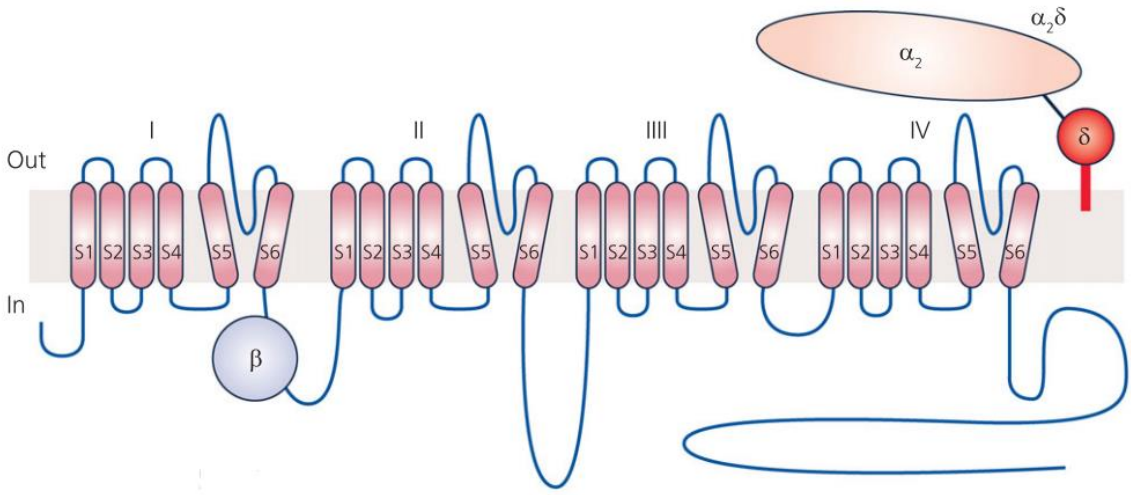

Figure 1: **Topology of a voltage gated calcium channel.** The pore forming α_1 subunit consists out of four homologues repeats, which are individually formed by six transmembrane domains S1-S6. The four repeats are connected via a link from S6 to S1. This linker connecting repeat one and two carries the α interaction domain (AID) at which the β subunit can bind. S4 of each repeat is more positively charged and therefore acts as the voltage sensor. The $\alpha_2\delta$ is anchored into the plasma membrane via a GPI anchor and the individual α_2 and δ subunits are connected via a GPI anchor (King, 2007). Figure from (Dolphin, 2016).

1.3 The Dmca1D voltage gated calcium channel

The Dmca1D is the L-type voltage gated calcium channel of *Drosophila* and was first cloned in 1995. It shares 78.3% sequence homology to the rat brain type D α_1 subunit, which is now called $Ca_v1.3$. The main differences of Dmca1D as compared to vertebrate calcium channels are its much longer C- and N-termini (Zheng et al., 1995). Structurally, the Dmca1D channel falls into the class of dihydropyridine sensitive calcium channels, but sequencing data show a non-conserved change in its IIS6 and IVS6 which may explain the unsensitivity to dihydropyridines. However, binding of phenylalkylamines (Verapamile, Gallopamil & Fendiline) is suggested (Zheng et al., 1995). Also conceivable from the sequencing data is heavily alternative splicing of the channel. To date there are 10 annotated splice variants which can be divided into two groups, five with a long and five with a short N-terminus (Flybase). In addition to splicing, posttranscriptional modifications further increase channel diversity. The Dmca1D channel has 2 possible glycosylation sites and 56 possible phosphorylation sites (8 for cAMP, 21 for protein kinase C and 27 for casein kinase), which together with alternative splicing and different $\alpha_2\delta$ and β subunit binding gives rise to a large amount of channel isoforms. *In situ* hybridization and Northern Blots show a high expression of the Dmca1D channel in the embryonic nervous system and adult heads (Zheng et al., 1995), and subsequent studies showed that the Dmca1D channel is the main calcium channel in embryonic and larval muscles (Eberl et al., 1998; Hara et al., 2015; Ren et al., 1998). Currently two mutants of the Dmca1D exist: the $Dmca1D^{X10}$ mutant, which affects the IVS4 of the α_1 subunit and is embryonic lethal because the larvae cannot hatch and the hypomorphic $Dmca1D^{AR66}$ affecting IS1 α_1 subunit (Eberl et al., 1998; Ren et al., 1998). The Dmca1D channel is also proposed to be involved in fluid transport. AR66 mutants often cannot inflate their wings (Eberl et al., 1998; Ren et al., 1998) and applying L-Type calcium channel blockers verapamil and nifidepine reduces fluid transport in Malpighian renal tubes (MacPherson et al., 2001). Heat inducible transgenic expression of the funnel web spider toxin ω-ACTX-Hv1a phenocopy the AR66 mutant, providing another potential blocker of the Dmca1D channel (Tedford et al., 2007). The AR66 mutant as well as an RNAi against the Dmca1D channel were used to show that Dmca1D is the major contributor of voltage dependent calcium influx into the identified larval crawling motoneurons aCC and RP2 and influences the firing properties of a neuron (Worrell and Levine, 2008). We could directly show the localization of the Dmca1D channel to patches of dendrites and the

axon of larval crawling motoneurons where it functions synergistically to enhance motoneuron firing output (Kadas et al., 2017). Dendritic Dmca1D channels amplify synaptic input and axonal Dmca1D channels increase burst duration and maximum intraburst firing frequencies during crawling. Firing frequencies are increased by interactions of Dmca1D with the calcium activated potassium channel slowpoke, which enables a fast after-hyperpolarization and therefore de-inactivates sodium channels faster (Kadas et al., 2015, 2017). Other studies also show a strong interaction of Dmca1D and slowpoke in presynaptic homeostatic plasticity, but restrict the function of Dmca1D only to the postsynaptic site, even though they used the AR66 mutant, which also reduces the function of presynaptic Dmca1D (Lee and Wu, 2010; Lee et al., 2008, 2014). In addition to its functions in motoneurons, the Dmca1D channel has been demonstrated in large and small ventrolateral neurons of the *Drosophila* brain expressing the PDF neuropeptide. In these neurons Dmca1D is regulated by the Dstac protein which influences the regulation of circadian rhythm by PDF.

This study reveals the presynaptic localization and function of Dmca1D in larval crawling motoneurons. We utilize *Drosophila* genetics, immunocytochemistry, electrophysiology, and optogenetics to uncover its precise subsynaptic localization, the amount of action potential-induced calcium influx into the presynaptic terminal through Dmac1D, its contribution to vesicle release, short term plasticity and synaptic vesicle endocytosis. Furthermore, we reveal its interaction with a presynaptic, membrane bound calcium ATPase (PMCA) to protect the active zone from additional calcium sources and keep release probability in a suitable range.

1.4 Membrane bound calcium ATPase PMCA

Reliable activity induced intracellular calcium signaling only functions with low cytosolic baseline calcium concentrations. Therefore, and because elevated calcium concentrations are toxic for the cell (Bagur and Hajnóczky, 2017), calcium clearance in excitable cells is a fundamental process to maintain cellular homeostasis. Key for maintaining intracellular calcium concentrations are calcium extrusion pumps, like the plasma membrane natrium/sodium exchanger (NCX), mitochondrial calcium uniporter, sacro/endoplasmic reticulum calcium ATPase (SERCA) and the plasma membrane calcium ATPase (PMCA). They all exhibit different affinities and capacities, while the PMCA is especially capable of fine tuning internal calcium concentrations (Krebs, 2017). The PMCA is a member of the P-type calcium pumps and its closest relative is

the SERCA pump. The name P-type originates from their ability to catalyse phosphorylations (Pedersen et al., 2007). In vertebrates 4 different genes (ATP2B1-4) encode PMCA1-4 which can generate 20 different isoforms by alternative splicing. The PMCA is a transmembrane protein composed of ten transmembrane helices, with the N- and C-terminus both located in the cytosol (Krebs, 2017). Most of the PMCA protein is highly conserved among the different isoforms except their C-termini, which differ between isoforms and give rise to unique properties of the respective protein (Calì et al., 2017; Islam, 2020; Krebs, 2017). PMCAs underlie a high affinity, low capacity calcium extrusion mechanism while extrusion speed can be adapted on a millisecond timescale (Lnenicka et al., 2006). A unique feature of PMCA pumps, what sets them apart from other P-Type pumps, is the autoinhibition mechanism. The C-Terminus of PMCAs exhibit a CAM binding site, which in the absence of CAM, binds a loop of the PMCA and keeps in autoinhibited (Lopreiato et al., 2014). Binding of CAM removes the C-Terminus and activates the pump. The duration of CAM binding results in a memory of the pump which depends on the properties of the C-Terminus and its CAM unbinding kinetics. The longer CAM binds, the longer lasts the memory and keeps the pump in a preactivated state, enabling fast reaction to consecutive calcium signals (Strehler et al., 2007). *Drosophila* has one gene encoding for the PMCA pump, which can generate 11 different isoforms. Like in vertebrates, these isoforms differ largely at their C-terminus, while the rest or the protein is almost identical (Flybase). Immunostaining revealed the presynaptic localization of PMCA in larval crawling motoneurons, where it is needed for calcium clearance after activity induced calcium influx (Lnenicka et al., 2006) but due to high postsynaptic PMCA levels, presynaptic immunostaining is imprecise to some extent.

Using different genetic tools, immunocytochemistry with subsequent deconvolution, electrophysiology and calcium imaging, we uncover the precise subsynaptic localization of the PMCA in the presynaptic terminal. Clustering of PMCA to subcellular compartments is consistent with other studies from T-helper cells (Korthals et al., 2017; Quintana et al., 2011) where PMCA augments calcium dependent processes in specific subcellular microdomains. Additionally, we show its function during action potential induced activity and for the control of evoked and spontaneous synaptic vesicle release.

1.5 Synaptic vesicle Endocytosis

Presynaptic terminals are highly specialized cell compartments that ensure tight temporal coupling of action potential invasion and calcium dependent neurotransmitter release. Therefore, VGCC that induce synaptic transmission and synaptic vesicles must be in close spacial proximity (Llinás et al., 1992), which is ensured by different scaffolding proteins (Petzoldt et al., 2016). The area in which VGCC and synaptic vesicles are bound together and where vesicles are released is called the active zone (Petzoldt et al., 2016). Because neurons have to operate over wide ranges of activity regimes and sometimes over long periods, two challenges are associated with sustained synaptic vesicle release. First, even though most synapses possess different pools of synaptic vesicles, which differ in size and their proximity to the active zone, *de novo* production of new synaptic vesicles in the soma would take too long and would require too many resources. Second, because the mean diameter of a synaptic vesicle at the *Drosophila* NMJ is about 34.4nm (Qu et al., 2009), fusion of a single synaptic vesicle with the presynaptic terminal adds roughly 3700nm² of membrane to the presynapse, sustained synaptic activity without membrane retrieval and recycling would increase the presynaptic membrane area, alter membrane tension and misalign pre- and postsynaptic structures (Kononenko and Haucke, 2015). Therefore, local synaptic vesicle endocytosis is critically required to maintain structural integrity and SV supply, and thus, to maintain synapse function even during prolonged and strong activity. To date, four different modes of SV recycling have been described, which operate at different time courses, involve at least partially different molecular components and differ in their efficacy in maintaining SV identity (Kononenko and Haucke, 2015). These include “kiss and run” endocytosis, clathrin mediated endocytosis, ultrafast endocytosis and bulk endocytosis.

Kiss-and-run exo-endocytosis is characterized by the transient formation of a fusion pore between SV and presynaptic membrane at the presynaptic active zone without SV collapse (Klingauf et al., 1998; Stevens and Williams, 2000). This mode is fast (<1s) and characterized by a transient fusion of vesicle and presynaptic membrane without full collapse of the SV and therefore circumventing sorting of vesicle membrane and proteins after reuptake of vesicle membrane (Murthy and Stevens, 1998). Therefore, it preserves vesicle identity in terms of one SV being the same before and after release and ensures fast recycling rates. What is not preserved during Kiss-and-run endocytosis is the vesicle´s identity in terms of a vesicle being equipped with the right

amount of synaptic vesicle proteins e.g. calcium sensors, which are necessary for reliable vesicle exocytosis. During each round of Kiss-and-run some vesicle proteins will diffuse into the presynaptic membrane (Wienisch and Klingauf, 2006) which will make exocytosis more and more imprecise if no other endocytic mechanism, which equips the SV with the right amount of SV proteins, would exist. Kiss-and-run recycling has been demonstrated in endocrine cells (Wu et al., 2014). Capacitance measurements (Xu et al., 2008) and high speed quantum imaging (Zhang et al., 2009) support kiss-and-run recycling in neurons, but its occurrence under physiological activity is hotly debated (Granseth et al., 2009; Kononenko and Haucke, 2015).

Clathrin mediated endocytosis (CME), probably the best described endocytotic pathway, has been demonstrated in many neurons, and operates at a slow time course (10-20s). It involves the uptake from the neuronal membrane surface by clathrin-coated vesicles after full fusion of the vesicle with the presynaptic membrane during exocytosis. Recent studies show, that the initiation of endocytosis is both calcium and clathrin independent. It was shown, that upon high sucrose stimulation endocytic pits are retrieved and that the pit formation is induced by membrane tension. However, endocytic pits stayed in the periactive zone without calcium and clathrin (Chanaday and Kavalali, 2020; Orlando et al., 2019). This indicates that the initiation of endocytosis is calcium and clathrin independent, while further progression of endocytosis is not. However, blockade of CME does not completely abolish SV recycling at the Drosophila NMJ (Heerssen et al., 2008), in *C. elegans* (Sato et al., 2009), or in hippocampal neurons (Kononenko et al., 2014). This suggests that neurons can capitalize on clathrin dependent and clathrin independent modes of endocytosis. This is further supported by the occurrence of more than one time constant in measurements of single vesicle recycling (Gandhi and Stevens, 2003).

Ultrafast endocytosis (UFE) has first been reported in *C. elegans* (Watanabe et al., 2013a) and then confirmed in mouse hippocampal neurons (Watanabe et al., 2013b) by stimulus triggered rapid high pressure freezing EM following optogenetic initiation of presynaptic action potentials. UFE is very fast (50-100ms), occurs after full fusion of the SVs during exocytosis and is characterized by large membrane invagination of the size of about 4 vesicles that take place outside the active zone. Importantly, it has been estimated that UFE comprises the predominant mode of endocytosis in mouse hippocampal neurons (Gan and Watanabe, 2018; Watanabe and Boucrot, 2017; Watanabe et al., 2013b). Ultrafast membrane retrieval does not depend on the

presence of clathrin, thus indicating that UFE may be a mechanism for fast restoral of presynaptic surface area at high stimulation frequencies. But note that during UFE, the rapidly retrieved large endocytotic vesicles transition into a “synaptic endosome” after about 1s, which is then coated by clathrin to regenerate new synaptic vesicles (Watanabe et al., 2014). Therefore, in the absence of clathrin, UFE can still retrieve membrane, but it cannot regenerate SVs for another round of release.

Bulk endocytosis, which has been found upon strong stimulation, such as chemical stimulation or bursts with hundreds of APs, is likely slow, and is characterized by large membrane invaginations distal from the active zone, which ultimately lead to large endocytotic vacuoles (Holt et al., 2003). These vacuoles are finally converted into smaller vesicles by yet mostly unknown mechanisms. Some authors have suggested that bulk endocytosis may be a rescue mechanism to effectively clear release sites during excessive activity (Kononenko and Haucke, 2015). To date, it is also not clear how bulk endocytosis and UFE are related to each other. Bulk endocytosis has been described in numerous systems, including the Drosophila NMJ, but UFE has only been demonstrated in *C. elegans* and mice.

Ideally the rates of SV exocytosis and endocytosis are matched (Haucke et al., 2011), but SV endocytosis operates much slower (from ~50ms to >20s) than SV exocytosis (~1ms). At high firing rates neurons can replenish the readily releasable pool of SVs from a reserve pool, but over time, recycling rates must be adjusted to maintain presynaptic homeostasis (membrane area and SV number). Consequently, means for the precise regulation of SV endocytosis rates must exist (Haucke et al., 2011). The intracellular Ca^{2+} concentration in the presynaptic terminal is discussed as a top candidate for this regulation. However, both the entry path for Ca^{2+} as a regulator of SV endocytosis, and the precise role of Ca^{2+} in endocytosis regulation remain incompletely understood (Haucke et al., 2011; Hosoi et al., 2009; Kononenko and Haucke, 2015; Leitz and Kavalali, 2015; Yamashita, 2012).

More than 40 years ago, induction of SV exocytosis in the absence of neural activity by bath application of the spider toxin, latrotoxin, revealed a physical enlargement of motoneuron axon terminals at the frog neuromuscular junction in the absence but not in the presence of extracellular Ca^{2+} (Hurlbut and Ceccarelli, 1974). This indicated a necessity for Ca^{2+} to recycle SV membrane. Since then, numerous studies employing different techniques in different animal systems have largely confirmed a role for Ca^{2+}

in SV endocytosis (Leitz and Kavalali, 2015), although considerable debate remains about the precise function of Ca^{2+}. Regulation of SV endocytosis by intracellular Ca^{2+} seems intuitively plausible to facilitate vesicle recycling upon increased neuronal activity. However, the Ca^{2+} concentrations required for endocytosis (~20µM) (Thomas et al., 1994) are much lower than those for exocytosis (200µM and higher in the AZ) (Cousin and Robinson, 2000). Moreover, all known endocytosis modes (see above) follow a much slower time course than exocytosis. Therefore, the time and concentration requirements for Ca^{2+} signaling differ markedly during SV endo- and exocytosis, which might require functional separation. Indeed, at the larval Drosophila neuromuscular junction (NMJ), evidence exists for regulation via two different Ca^{2+} channels (Kuromi et al., 2004). There, the Ca_V2 homolog, Dmca1A, localizes to the active zone and is critically required for exocytosis, but not for endocytosis. By contrast, inorganic Ca^{2+} channel blockers that do not block Dmca1A, reduced endocytosis but left exocytosis unaffected, thus indicating that separate channels mediate Ca^{2+} dependent SV release and recycling (Kuromi et al., 2004). FM2-10 measurements of synaptic vesicle pools at the mouse NMJ support the idea of L-Type (Ca_V1) VGCCs being necessary to recycle synaptic vesicles into a high release probability pool but have no effect on synaptic transmission (Perissinotti et al., 2008). At the Drosophila NMJ, it has been suggested that a novel Ca^{2+} channel, named flower, regulates SV endocytosis. The idea is that flower channels localize to the SV membrane and become functional in the presynaptic membrane upon vesicle fusion. The more SV fusion, the higher the likelihood of functional Ca^{2+} channel formation in the presynaptic membrane (Yao et al., 2009, 2017), but this model has so far not been further confirmed in any other preparation or by other labs at the Drosophila NMJ.

Therefore, the calcium source for activity dependent endocytosis regulation, as well as the mechanisms that allow parallel calcium signaling for exo- and endocytosis without mutual interference of the calcium signals, remain elusive. This thesis will address this problem, identify the entry routes of calcium during AP-triggered exo- and endocytotic regulation and provide a new mechanism that ensures stable release probability in the limited space of presynaptic terminals.

1.6 Hypotheses

This thesis will test the following hypotheses:

I. Two distinctly different VGCCs with different kinetics, conductances and subsynaptic localization are used for separate regulation of exocytosis (Dmca1A / Ca_V2) versus endocytosis (Dmca1D / Ca_V1)
II. The Dmca1D (Ca_V1, L-type) channel is not required for SV exocytosis but modulates short term plasticity
III. AP-triggered calcium influx through Dmca1D facilitates synaptic vesicle endocytosis
IV. The PMCA protects the active zone from external calcium sources and separates Ca_V2 and Ca_V1 channel function in the minimal space of the presynaptic terminal

Based on our hypotheses we make the following predictions:

I. Knockdown or knockout of Dmca1D has no effect on evoked synaptic transmission
II. Knockout of Dmca1A abolishes synaptic transmission
III. Knockdown of Dmca1D causes decreased AP-triggered calcium influx into the presynaptic terminal
IV. Knockdown of Dmca1D alters short-term plasticity of synaptic transmission
V. Knockdown of Dmca1D reduces the rates of synaptic vesicle endocytosis and thus causes increased synaptic depression
VI. PMCA protects active zones from AP-triggered calcium influx through Dmca1D, and thus, knockdown of PMCA causes increased AP-triggered calcium signals in the active zone and consequently increases evoked synaptic transmission
VII. These effects of PMCA knockdown can be rescued by concomitant knockdown of Dmca1D
VIII. Knockdown of PMCA increases spontaneous SV release
IX. Knockdown of PMCA in motoneurons causes muscle spasm

2. Material and Methods

2.1 Flies

Drosophila melanogaster were reared at 25°C and 60 % humidity under a 12-hour light:dark cycle. For experiments, third instar larvae of both sexes were used. We used UAS-RNAi transgenes to knockdown Ca_v1 channels, or PMCA, or both under the control of the motoneuron GAL4 driver $vGlut^{OK371}$ (Mahr and Aberle, 2006). We used CantonS wildtype animals and the genetic background of the respective knockdown genotypes as controls, but without the UAS-RNAi constructs. For calcium imaging $vGlut^{OK371}$-Gal4 and the respective knockdown were recombined with different versions of GCaMP6 (Bloomington stocks 42747, 77131, and this work). To create animals with Ca_v1 null mutant motoneurons, mosaic analysis with a repressible cell marker (MARCM)(Lee and Luo, 2001) was employed as previously described (Kadas et al., 2017; Klein, 2016). The knockdown effectiveness of the UAS-RNAi transgene for the Drosophila Ca_v1 homolog, Dmca1D (Bloomington stock 33413, HMS00294), has previously been shown to yield a knockdown efficacy of ~80% (Kadas et al., 2017; Klein, 2016). The TRiP.HMS00294 RNAi transgene has been targeted with a VALIUM vector (Vermillion-attB-loxP-Intron-UAS-MCS) to the attP-landing site on the third chromosome(Ni et al., 2009). As genetic control, the same VALIUM vector has been inserted at the same attP landing site in the same genetic background, but without Ca_v1 RNAi (Bloomington stock 35786) (Ni et al., 2008). The UAS-PMCA-RNAi line KK108105 was received from the Vienna Drosophila Research Center (stock # v101743) and was validated for the absence of a potentially detrimental insertion prior to use (Green et al., 2014). The PMCA protein trap line PMCA[CPTI001995] (Lowe et al., 2014) was provided by the Kyoto stock center (stock #115256). The muscle-specific line C57-Gal4 was described by(Koh et al., 1999). The UAS-GFP-RNAi line and the UAS- {UAS-Nslmb-vhhGFP4}2 line (Caussinus et al., 2012) were received from the Bloomington Stock Center (#9330, #38422). See table 1 for a list of all genotypes used with reference to the different experiments conducted in this study.

2.1.1 Fly Stocks

Table 1*:* Genotypes and Origin of used *Drosophila melanogaster* flies

genotype	phenotype	experiment
Canton S	wildtype control	TEVC
y1sc* v1/UAS-Dcr2; OK371-GAL4/+; P{TRiP.HMS00294}attP2/+	Ca_v1 RNAi in motoneurons	TEVC, CC, FM1-43 imaging, behavior
y1 v1/AUS-Dcr2; OK371-GAL4/+; P{UAS-GFP.VALIUM10}attP2/+	control for Ca_v1 RNAi in MNs	TEVC, CC, FM1-43 imaging, behavior
w1118/UAS-Dcr2; OK371-GAL4/+; P{TRiP.HMS00294}attP2/+	Ca_v1 RNAi in motoneurons	morphometry
w1118/UAS-Dcr2; OK371-GAL4/ P{attP,y+,w3 KK108105}VIE-260B; +/+	PMCA RNAi in motoneurons	TEVC, behavior, morphometry
w1118/UAS-Dcr2; OK371-GAL4+; +/+	control for PMCA RNAi in motoneurons	TEVC, behavior, morphometry
w1118/UAS-Dcr2; OK371-GAL4/ P{attP,y+,w3 KK108105}VIE-260B; P{TRiP.HMS00294}attP2/+	Ca_v1 and PMCA RNAi in motoneurons	TEVC, behavior, morphometry
cacFLP STOP ND/Y;OK6-GAL4/FLP;+	Ca_v2 mosaic knock out	TEVC
cacFLP STOP ND/Y;OK6-GAL4/+;+	control for mosaic knock out	TEVC
w1118/+; OK371-GAL4/+; mhcP-myrGcamp6m/+	control	Ca^{2+} imaging in muscle
w1118/+; OK371-GAL4/ P{attP,y+,w3 KK108105}VIE-260B; mhcP-myrGcamp6m/+	PMCA RNAi in motoneurons	Ca^{2+} imaging in muscle
w1118/+; OK371-GAL4/+; mhcP-myrGcamp6m/ P{TRiP.HMS00294}attP2	Cav1 RNAi in motoneurons	Ca^{2+} imaging in muscle
w1118/+; OK371-GAL4/ P{attP,y+,w3 KK108105}VIE-260B; mhcP-myrGcamp6m/ P{TRiP.HMS00294}attP2	PMCA and Cav1 RNAi in motoneurons	Ca^{2+} imaging in muscle
w;UAS-brp.S-mCherry-GCaMP6s $vGlut^{OK371}$-GAL4/+	control	Ca^{2+} imaging in presynaptic AZs
w;UAS-brp.S-mCherry-GCaMP6s $vGlut^{OK371}$-GAL4/+; P{TRiP.HMS00294}attP2/+	Ca_v1 RNAi in motoneurons	Ca^{2+} imaging in presynaptic AZs
w;UAS-brp.S-mCherry-GCaMP6s $vGlut^{OK371}$-GAL4/UAS- P{attP,y+,w3 KK108105}VIE-260B;+/+	PMCA RNAi in motoneurons	Ca^{2+} imaging in presynaptic AZs
Cac[NT27]; +; +	Temperature sensitive Ca_v2 channel mutant	Current clamp/behavior

y1sc* v1/Dcr2; OK371-GAL4i/ P{20XUAS-IVS-GCaMP6f} attP40; P{TRiP.HMS00294}attP2/+	Ca_v1 RNAi in motoneurons	Ca2+ imaging of boutons
y1 v1/Dcr2; OK371-GAL4i/ P{20XUAS-IVS-GCaMP6f} attP40; P{UAS-GFP.VALIUM10}attP2/+	control for Ca_v1 RNAi in MNs	Ca2+ imaging of boutons
C57-Gal4/+; PMCA[CPTI001995]/+	Endogenous PMCA tagged with Venus	PMCA localization
C57-Gal4/UAS-GFP-RNAi; PMCA[CPTI001995]/+	Depletion of postsynaptic PMCA-Venus	PMCA localization
UAS-Nslmb-vhhGFP4/+; C57-Gal4/UAS-GFP-RNAi; PMCA[CPTI001995]/+	Depletion of postsynaptic PMCA-Venus	PMCA localization
+/UAS-PMCA-RNAi; C57-Gal4/+	Postsynaptic PMCA RNAi	PMCA localization + kd
OK371-Gal4/UAS-PMCA-RNAi; C57-Gal4/+	Pre-and Postsynaptic PMCA RNAi	PMCA localization +kd
y1w* P{hsFLP}1; b1 Ca-α1DX10 pr1 P {neoFRTry+}40A/ P{tubPGAL80}LL10 P{neoFRT}40A, P{UAS-mCD8::GFP.L}Ptp4ELL4; P{tubP-GAL4}LL7)	Mosaic Cav1 null mutant with a repressible marker (MARCM)	CC
w1118;OK371-Gal4/UAS-BRPshort(D3)-strawberry; mhc Pmyr GCaMP6m/+	Presynaptic labeled Brp and postsynaptic GCaMP	Co-labeling of AZs and postsyn. Ca2+ imaging

2.1.2 Larval Preparation

Third-instar larvae were dissected in HL3.1 saline (see2.2.1). Larvae were pinned dorsal side up in sylgard-filled Petri dishes with pins through the mouthhooks and the tail. They were then dissected along the dorsal mid-line, and the dorsal cuticle and muscles were stretched laterally and pinned down with two pins on each side. After removing the gut and esophagus and the ventral nerve cord (VNC) the whole larvae was viewed under the microscope (Olympus BX51WI) with a 20 X water immersion lense.

2.2 Solutions

2.2.1 HL3.1 Saline

We used this modification of the hemolymph-like HL3 saline (Stewart et al., 1994) which was especially designed for recordings at the *Drosophila* neuromuscular junction and increases longevity of the preparation(Feng et al., 2004). Composition in mM: NaCl 70, KCl 2.5, $MgCl_2$ 2, $CaCl_2$ 0.5, $NaHCO_3$ 10, trehalose 5, sucrose 115, HEPES 5, (pH adjusted to 7.24-7.25 with 1N NaOH, mOsm: 300-310)

2.2.2 Normal Saline

In the course of a study about the anatomy and physiology of the *Drosophila* neuromuscular junction this saline was developed (Jan and Jan, 1976). It is composed of mM: NaCl 128, KCl 2, $MgCl_2$ 4, $CaCl_2$ 1.8, sucrose 35.5, HEPES 5 (pH adjusted to 7.24-7.25 with 1N NaOH, mOsm: 300-310)

2.2.3 High Potassium Saline

To induce action potential firing without nerve stimulation, we used high concentrations of potassium (20mM) that results in potassium flowing into the cell, also leads to membrane depolarization and action potential firing. For adequate image acquisition, nerve terminals should stay in place. Therefore, we added 7mM of Glutamate to prevent the muscles from contracting. To prevent too high osmolality, all other components had to be adjusted. Full composition of high potassium saline is in mM: NaCl 108, KCl 20, $MgCl_2$ 4, $CaCl_2$ 2, Glutamate 7, sucrose 35.5, HEPES 5 (pH adjusted to 7.24-7.25 with 1N NaOH, mOsm: 320)

2.2.4 Calcium-free Saline

In order to dissect larvae for FM1-43 imaging we used calcium-free saline with normal amounts of potassium. Full composition of calcium-free saline is in mM: NaCl 108, KCl 2, $MgCl_2$ 4, $CaCl_2$ 0, Glutamate 7, sucrose 35.5, HEPES 5 (pH adjusted to 7.24-7.25 with 1N NaOH, mOsm: 320)

2.3 Two Electrode Voltage Clamp

All Two Electrode Voltage Clamp (TEVC) recordings were performed in HL3.1 saline with either 0.5 or 2mM external Ca^{2+}. Experiments were performed on third-instar larval NMJs (muscle 6&7 abdominal segments A2/A3, $Cac^{FLP\ STOP}$ recordings were conducted on muscle12 in abdominal segments A2/A3).The respective nerve was sucked in with a self-built suction electrode (Johnson et al., 2007) which was filled with HL3.1 saline. Subsequently, the nerve was stimulated for 0.1ms to trigger action potential firing (voltage was stepwise increased until the first synaptic transmission could be recorded, from that voltage, 1V was added to reliably evoke APs).For EGTA-AM experiments larvae were first dissected in Ca^{2+} free HL3.1 saline then incubated for 10min in Ca^{2+} free HL3.1 saline containing 25µM EGTA-AM (Invitorgen, Catalog #E1219). After the 10min incubation preparations were washed in HL 3.1 saline (0.5mM Ca^{2+}) three times and then recorded. Recordings were only further considered from cells with an initial V_m below -50mV using intracellular electrodes filled with 3M KCl with resistances of 8-10MΩ (Electrodes for current injection) and 20-25MΩ (Electrodes for measuring the membrane voltage). Both electrodes were pulled from Borosilicate glass microelectrodes with filament (OD1 mm, ID 0.5mm; Molecular Devices Sutter Instrument USA) with a Flaming/Brown Puller Model P-97 (Sutter Instruments USA). Excitatory postsynaptic currents (EPC) were evoked by an Isolated Pulse Stimulator (Model 2100 A-M Systems USA), recorded at a clamped voltage of -70mV with a sampling rate of 50kHz and filtered with the anti-alias filter at 25kHz using the AxoClamp 2B amplifier (Molecular Devices Axon Instruments USA). Data analysis was done with Clampfit 10.7. Traces were first filtered with a 360Hz Gaussian low pass filter, then template searches were run over the trace for single pulses, paired pulses and spontaneous miniature excitatory postsynaptic currents (mEPSCs or Minis). The resulting files were used to analyze amplitude, half width and area. Rise and decay tau were measured with an one-term exponential product fit (Levenberg-Marquadt method with a max of 5000 iterations).

2.4 Calcium Imaging

To determine the amount of calcium influx through the Dmca1D channel into cellular or subcellular compartments, we utilized the genetically encoded fluorescent Ca^{2+} indicator GCaMP (Nakai et al., 2001) to measure Ca^{2+} influx upon action potential invasion. A GFP-based florescence protein cpEGFP, which is connected to the Ca^{2+} binding protein calmodulin (CaM) and the CaM-binding peptide M13, forms the calcium indicator GCaMP. In a Ca^{2+} free environment, GCaMP has weak fluorescence. Upon binding of Ca^{2+} to CaM the interaction of CaM and M13 result in a conformational shift in the cpEGFP. We specifically used the versions GCaMP6f, m and s (Chen et al., 2013) which distinguish from each other by their calcium binding kinetics that result in different fluorescence rise and decay times. Upon action potential induced activity (20Hz for 2 seconds) at the *Drosophila* NMJ GCaMP6f, m and s binding properties are:

Table 2: Florescence properties of GCaMP6f, m and s according to Chen et al. 2013

	Rise time,t_{peak} (s)	Decay time,$t_{1/2peak}$ (s)
GCaMP6f	0.14	0.4
GCaMP6m	0.14	0.8
GCaMP6s	0.16	1.2

2.4.1 Presynaptic Calcium Imaging

To measure the overall calcium influx through the Dmca1D channel into presynaptic terminals, cytosolic expression of GCaMP6f was expressed under the control of $vGlut^{OK371}$ GAL4 driver that drives expression of UAS-transgenes in glutamatergic neurons and therefore motoneurons. To block calcium influx through Dmca1D we used RNAi knockdown to prevent the protein from being translated and we used the biogenic amine Tyramin (10^{-5}M) to selectively block the Dmca1D channel (Schützler et al., 2019). Recordings were performed in HL3.1 saline with 0.5mM Ca^{2+} and 7mM Glutamate concentration to prevent muscle twitches. Larvae were dissected as described in 2.1.3 and mounted under an upright Zeiss Axio Examiner A1 epifluorescence microscope with a Hamamatsu Orca Flash 4.0LT Model C11440-42U CMOS camera and a 40x water immersion lens. Image acquisition rate was 30ms exposure time. Electrical nerve stimulation was the same as for TEVC, except that we consistently used a stimulus duration of 0.5ms and 6V to ensure reliable action potential generation. With these settings, 10 action potentials at 50Hz were presented

to the presynaptic terminal. The NanoJ core plug-in (Laine et al., 2019) was used to correct for remaining movement in the xy plane. Image stacks that moved in z were excluded from the analysis. Region of interest was the circumference of the bouton. Background fluorescence was routinely subtracted. Raw data were exported to MS Excel, and ΔF/F was calculated by [F(stim)-F(rest)]/F(rest)] (Schützler et al., 2019). F(rest) was determined as the mean fluorescence calculated from 100 frames before any stimulation. Net bouton calcium influx was recorded in controls and with Ca_v1 channel knock down in motoneurons

2.4.1.1 Active Zone Calcium Imaging

To further determine the amount of calcium entering the active zone (AZ) through Dmca1A and Dmca1D upon AP invasion, we used a 60x water immersion lense and expressed the UAS-brp.S-mCherry-Gcamp6s transgene, where GCaMP is bound to the scaffolding protein bruchpilot (brp), under the control of the $vGlut^{OK371}$ GAL4 driver. Electrical nerve stimulation was also done with a stimulus duration of 0.5ms at 6V, but at 100Hz for 150ms resulting in 15AP. The NanoJ core plug-in (Laine et al., 2019) was used to correct for remaining movement in the xy plane. Image stacks that moved in z were excluded from the analysis. Regions of interest were placed on 5 active zones per bouton and fluorescence intensities were measured over time. Raw data were exported to MS Excel, and ΔF/F was calculated by [F(stim)-F(rest)]/F(rest)] (Schützler et al., 2019). F(rest) was determined as the mean fluorescence calculated from 100 frames before any stimulation. Net bouton calcium influx was recorded in controls and with Ca_v1 channel knock down in motoneurons.

2.4.2 Postsynaptic Calcium Imaging

For image acqusition an upright Olympus BX51WI with a 60x water-immersion objective with a CSU-X1 spinning disk (Yokogawa) and an EMCCD camera (iXon+897, Andor Technology) were used. Recordings were obtained in normal HL3.1 Saline in 0.5 and 2mM Ca^{2+}. For each Calcium concentration sponateous events with and without 1µM TTX and evoked responses without TTX were recorded. Spontaneous events were recorded with a aquestion rate of 20Hz over a duration of 250s (5000 frames). Image stacks were analyzed using custom-written routines in ImageJ/FIJI Software (NIH, USA). Prior to detection of individual active zones (AZs), acquired stacks underwent correction of XY drift using NanoJ plugin (Laine et al., 2019). Threshold-based automatic detection of regions of interest (ROIs) corresponding to

AZs included several steps. First, image calculation was performed for each acquired stack. For this purpose, intensity value in Z projection (average intensity for slices within 200 ms) was subtracted from the Z projection (maximum intensity) of the 2 following slices, with this operation being repeated for all slices in a sliding window manner and stored as a new stack. In the resulting stack with lower level of ambient fluorescence, the detection of local maxima as brightest pixels was performed (prominence level 6 standard deviations (SDs) calculated for the whole image) and circular selections were automatically drawn around each maximum (diameter 7 pixels, pixel size 233 nm) as a potential AZ. Next, mean fluorescence intensity within each circular ROI was calculated and ROIs with the mean intensity less than 6 x SDs were discarded from further analysis. For remaining ROIs, the temporal profile of activity (Z-axis profile) was extracted and tested for condition $F_{max} >= F_{base}+3xSDs$, where F_{base} is mean fluorescence within 400 ms just prior to the event and F_{max} is maximum fluorescence value within 200 s after the event's onset. Finally, each ROI fulfilling the latter criterion was classified as new if its center was more than 5 pixels away from already existing (detected earlier in given stack) ROIs. To test whether responses occurred in a quanta-like manner, the extracted events for each individual ROI were normalized to the minimal (smallest) response detected in given ROI. Histograms were generated using Graphpad Prism8.

2.5 FM1-43 Imaging

FM dyes are functional dyes which belong to the familiy of styryle dyes. They are characterised by a univalent radical C_6H_5-CH=CH- that is derived from styrene (Deligeorgiev et al., 2010). The fluorescent FM dyes are used to study endocytosis, vesicle pools and exocytosis in multiple systems (Verstreken et al., 2008). Characteristic for these dyes is their water solule head and a lipophilic tail. FM dyes vary in their fluorescence, which is determined by the central region that seperates hydrophilic head and lipophilic tail. To study vesicle exo- and endocytosis with and without the Dmca1D channel we used FM1-43 (N-[3-triethylammoniumpropyl]-4-[p-di-butylaminostyryl]pyridinium dibromide). Larvae were dissected in calcium-free saline with 7mM Glutamate (2.2.4) as described in 2.1.3 and mounted under a fixed upright Zeiss Axio Examiner A1 epifluorescence microscope with a 40x water immersion lens and imaged with an Orca Flash 4.0LT Model C11440-42U CMOS camera (Hamamatsu) controlled with HOKAWO 3.00 software. A first image was taken of

motoneuron boutons on M6/7 to determine resting fluorescence (F(rest)). Next, motoneuron activity and loading of FM1-43 into recycled synaptic vesicles was induced by perfusion with modified high potassium HL3.1 saline containing 0.5mM calcium, 20 mM potassium, and 2µM FM1-43, for 3 minutes. This was followed by washing for 3 minutes in calcium- and FM1-43-free normal HL3.1 saline. Immediately after washing, the second image was taken to determine fluorescence intensity in boutons after FM1-43 loading into recycled SVs (F(load)). Next the preparation was stimulated again by perfusion with 0.5mM calcium, 20 mM potassium saline and washed for additional 3 minutes in calcium-free normal salines. Immediately after washing, the third image was taken to determine fluorescence intensity in boutons after FM1-43 unloading during the release of loaded SVs (F(unload)). Background fluorescence was subtracted from all images. ΔF/F was calculated as [F(load)-F(rest)]/F(rest)] for loaded boutons and as [F(unload)-F(rest)]/F(rest)] for unloaded boutons. Experiments were conducted with Ca_v1 knock down in motoneurons and the respective controls.

2.6 Immunocytochemistry

Ca_v2 channel localization was assessed with endogenously tagged channels, for which correct localization was previously demonstrated (Gratz et al., 2019). Triple immunostaining was conducted with α-GFP (rabbit anti-GFP, Invitrogen, A11122) for tagged Ca_v2 channels, α-Ca_v1 (goat anti-Ca_v1, Santa Cruz, sc-32083, 1:200 in PBS), and the active zone marker bruchpilot (mouse α-Brp, nc82, DSHB, 1:200). Antibody specificity of sc-32083 for the Drosophila Ca_v1 homolog Dmca1D was previously demonstrated by Western blotting and immunocytochemistry in Dmca1D mosaic null mutant animals (Kadas et al., 2017). Larvae were dissected in saline, fixed for 5 minutes in ice cold ethanol (100%), washed 8 times 20 minutes in PBS (0.1 M) with 0.3 % TritonX and 5% bovin albumin serum (BSA) and 6 times 30 minutes in PBS-TritonX (0.5%) with 5% BSA. Then preparations were incubated with primary antibodies (rabbit anti-GFP, Invitrogen, A11122, 1:400; mouse anti-Brp, nc82, DSHB, 1:200; goat anti-Dmca1D, Santa Cruz, sc-32083, 1:400, all in PBS) overnight at 4°C in PBS-TritonX (0.1%). Following incubation with primary ABs preparations were washed 6 times 30 minutes in PBS and incubated in secondary ABs (donkey anti rabbit-Alexa-488, Jackson ImmunoResearch, Cat # 711-546-152; donkey anti mouse-Alexa 555, Thermo Fisher Cat # A-31570; donkey anti goat-Alexa 647, Jackson ImmunoResearch, Cat # 705-605-147; all 1:1000) over night at 4°C. Then preparations

were washed 6x30 minutes in PBS, dehydrated in an ascending ethanol series (50, 70, 90, 100%, 10 minutes each), cleared and mounted in methylsalicylate.

To compare presynaptic structure in controls and following PMCA knock down, or Ca_V1 knock down, or PMCA Ca_V1 double knock down, motoneuron axon terminal bouton structure was visualized with α-HRP (horse radish peroxidase, Jackson ImmunoResearch, Cat # 323-005-021, 1:500 in PBS). Presynaptic active zones (AZs) were labeled with α-NC82 (Brp), and glutamate receptor IIc (GluRIIc) was labeled by immunocytochemistry. Larval body walls were dissected in Ca^{2+}-free saline and further processed essentially according to Bellen and Budnik (2000) (see also https://bio-protocol.org/e3142 for a video documentation). Samples were fixed in phosphate-buffered 4% PFA for 30 minutes, all wash steps and antibody incubations were done with 0.1M phosphate buffer (pH 7.2) containing 0.2% Triton-X100. Following fixation, samples were co-incubated throughout, with incision marks used for unambiguous tracing of genotypes. Rabbit anti-GluRIIc (Kern et al., 2013) at 1:400 and mouse anti-Brp NC82 (Wagh et al., 2006) at 1:50 were incubated overnight at 4°C at 1: 50. Alexa 488-conjugated goat anti-rabbit, Alexa 568-conjugated goat anti-mouse and Alex 647-conjugated anti-Hrp antibodies (Jackson Laboratories) were applied at 1:300 for 4 h at room temperature. To enhance the Venus-signal associated with the PMCA protein-trap, an Atto488-conjugated FluoTag®-X4 anti-GFP nanobody (NonoTag Biotechnologies) was used at 1:300 for 2h at room temperature. Samples were mounted in Vectashield medium.

Image acquisition and processing: Immunolabeled NMJ whole mount preparations were scanned with Leica SP8 CLSM with a 40x oil immersion lens (NA 1.2) at zoom 3.5 at 1024 times 1024 pixels. The resulting xy- pixel size was 88nm and z-step size distance was 300nm (Ca_V1, Ca_V2, and Brp triple labels, Fig. 2). Alexa 488 was excited with an Argon laser at 488 nm and detection with a PMT between 500 and 530 nm. Alexa 555 was excited with a diode solid state laser at 561 nm and detection with a PMT between 570 and 600 nm. Alexa 647 was excited with a Helium-neon laser excitation at 633 and detection with a gallium arsenide hybrid detector between 640 and 690 nm. Alexa 488 and 647 were excited and scanned simultaneously, but Alexa 555 was scanned separately to avoid signal cross talk (SP8 sequential scan mode). Laser and detector settings were switched after each frame. Images were processed with AMIRA4.1, ImageJ, and Corel Draw X7 software. Alternatively, for morphometric analysis of NMJ structure following various RNAi knock downs, a Leica SP5 CLSM

with a 63x oil objective (NA 1.4) with zoom 2.5 was used and z-step distance remained 0.3µm. Settings were kept constant in each session. Wherever necessary, two overlapping frames were recorded to cover an entire NMJ. For morphometry, files were deconvolved using the express mode in Huygens Professional software (version 19.10.0; Scientific Volume Imaging) and were further processed using Imaris x64 (version 9.5; OXFORD Instruments). The surface tool was applied to Hrp-defined masks, with a gaussian filter set to 0.5 µm such that glutamate receptor fields were included. For measurements, surfaces were restricted to Brp/GluR-containing type Ib bouton areas by manual trimming in 3D. For counting of AZ, Brp signals were detected by automized spot detection with the estimated spot size diameter set to 0.15 µm. Intensity measurements were carried out on maximum projections of raw image stacks using the same surfaces as for morphometry to define ROIs. As Hrp mean intensities did not vary significantly between genotypes, they were used to normalize intensities for GluR and Brp for each NMJ individually to correct for variations associated with the Z-depth of samples on a given slide. For statistics, intensities were first normalized to controls for each staining session separately (4 sessions with 12 to 38 NMJs from 6 to 19 animals) and then pooled for further statistical analysis using GraphPad Prism7.

2.7 Statistics

Statistical analyses were done using Graphpad Prism Software (Version 8.3.1). Datasets were tested for normal distribution with the Shapiro-Wilk Test. Normally distributed data were then tested with Students t-test (for pairwise comparison). Normally distributed analysis for more than two groups was done with a one-way ANOVA and post hoc tested with a Tukey multiple comparison test. Non-normally distributed data sets of two groups were tested with Mann-Whitney U Test (pairwise comparison) and datasets with more than two groups were tested with a Kruskal Wallis ANOVA and post hoc tested with a Dunns multiple post hoc comparison test. For all datasets mean and standard error of mean (SEM) are shown. Significance levels were * $p<0.05$; ** $p<0.01$; *** $p<0.001$.

3. Results

3.1 Dmca1D is localized at presynaptic terminals of the *Drosophila* larval NMJ

We could show by immunocytochemistry that the Dmca1D L-type calcium channel localizes to presynaptic terminals of the *Drosophila* larval crawling motoneurons. Using the Cas protein Bruchpilot (Brp) as an active zone marker (Kittel et al., 2006), we find a strict spatial separation of the already described Ca_v2 channel homolog, Dmca1A, in the active zones where it triggers synaptic vesicle release upon action potential invasion (Kittel et al., 2006) and the Ca_v1 channel homolog, Dmca1D, outside the active zones (Fig. 2). Triple labeling for Dmca1A (Fig. 2Aii, green), Dmca1D (Fig. 2Bii, blue) and Brp (Fig. 2Ai and Bi, red) show colocalization of Dmca1A and Brp in active zones (Fig. 2A). Otherwise, Dmca1D expression is only found outside active zone and does not colocalize with Brp (Fig. 2B).

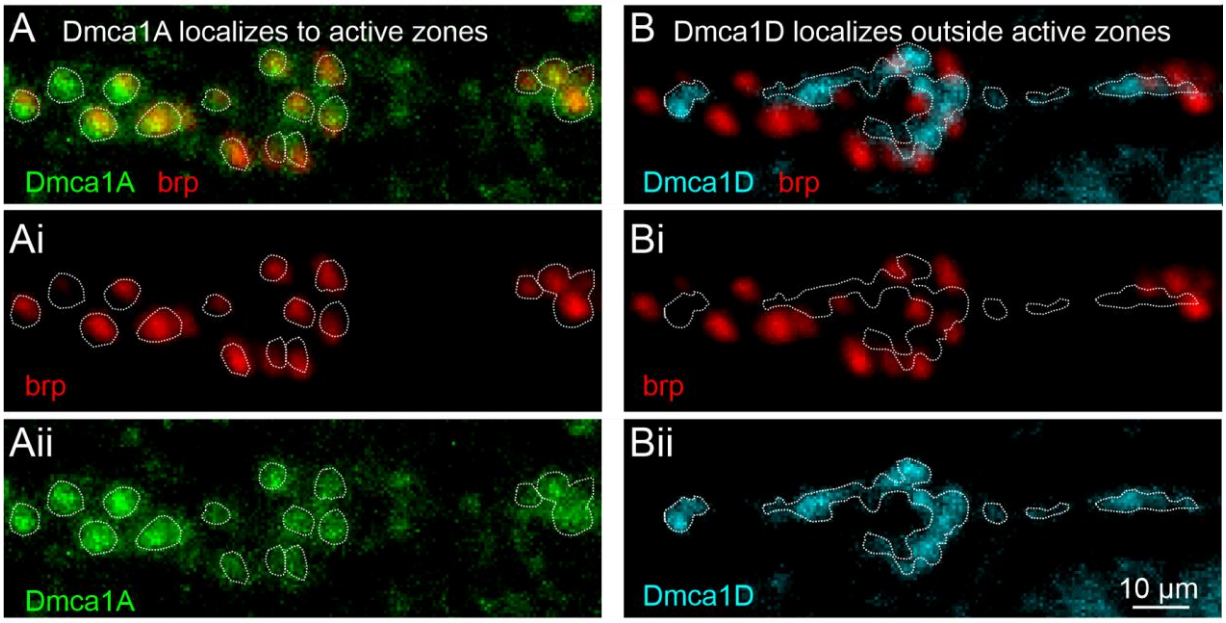

Figure 2: **Spatial separation of presynaptic VGCCs**. **A** double labeling of the Dmca1A channel (**Aii**, green, dotted white line) and the active zone marker Brp (**Ai**, red) show co-localization of both in active zones. **B** Antibody staining in the same preparation against Dmca1D (**Bi**i, blue, dotted white line) shows its location outside the active zone (**Bi,** red).

3.2 Dmca1D contributes up to 50% of the action potential induced calcium influx into the presynaptic terminal

After showing the localization of the Dmca1D channel to presynaptic terminals of *Drosophila* larval crawling motoneurons, we wanted to determine its relative contribution to action potential triggered calcium influx into the synaptic terminal. Cytosolic expression of the calcium indicator Gcamp6m reveales a 50% reduction of calcium influx into terminals in response to 10Hz stimulus trains with 10APs upon expression of Dmca1D RNAi in motoneurons as compared to control (Fig. 3 C&D).

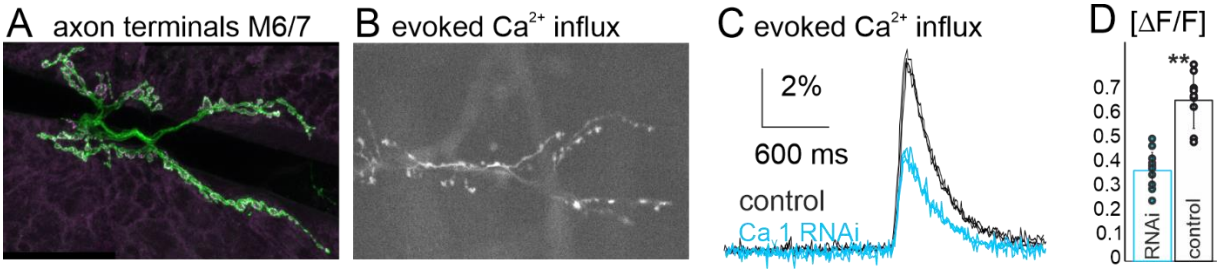

Figure 3: **Dmca1D mediates 50% of AP induced calcium influx into presynaptic terminals**. **A** Representative axon terminal projections (green) with Brp (magenta) and with expression of Gcamp6m (**B**). **C** Traces of action potential triggered calcium influx into presynaptic terminal after 10 AP at 10Hz in controls (black) and Dmca1D knockdown (blue). **D** quantification shows significant reduction of calcium influx after AP invasion in Dmca1D knockdowns.

To exclude developmental effects caused by the Dmca1D RNAi, which could possibly cause this effect, we analyzed bouton size and number of AZ in MN terminals at muscle fibre M4 in abdominal segments A2&3. Number of AZ was measured by counting Brp puncta. Dmca1D RNAi and control show no significant difference in number of AZs and surface area (Fig. 4A, B), resulting in the same AZ density (Fig. 4C, Ei, Fi). Hence, we can exclude major developmental defects on presynaptic structure by a knockdown of the Dmca1D channel which causes the previously described reduction of AP induced Gcamp6m fluorescence. Additionally, we analyzed immunofluorescence intensity of postsynaptic glutamate receptors (GluR) to exclude developmental defects on postsynaptic receptor expression in muscle upon presynaptic Dmca1D knockdown, which showed no significant difference between knockdown and control (Fig 4D, E, F).

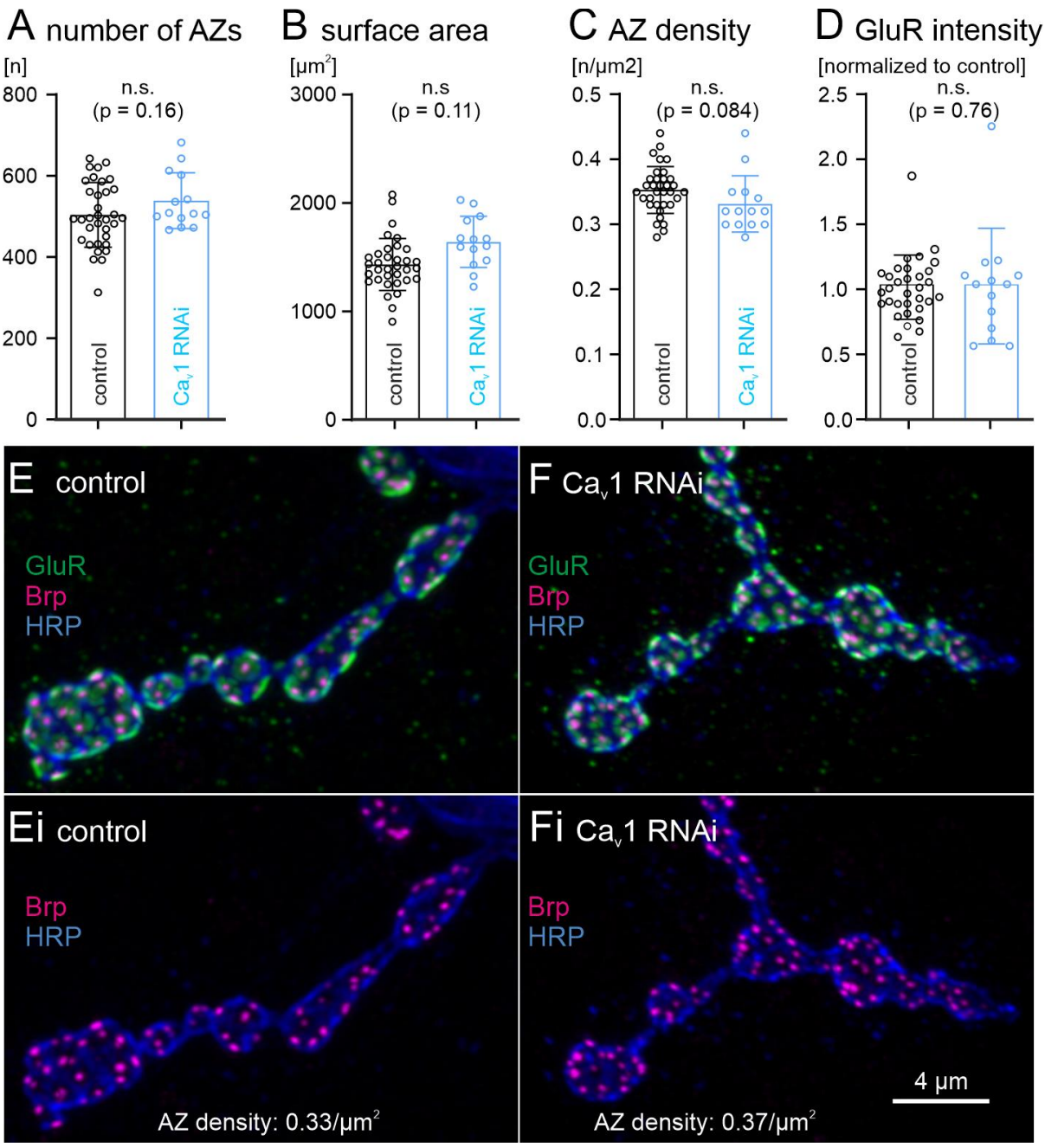

Figure 4: **Structural analysis of presynaptic terminals upon Dmca1D knockdown. A** Number of active zones (determined by Brp puncta) in control and Dmca1D knockdown show no significant difference (mean ± SD: control, 504 ± 80; Dmca1D -RNAi, 539 ± 69). **B** surface area of presynaptic terminals show a slight, but not significant increase in Dmca1D RNAi compared to control (mean ± SD: control, 1434 ± 241 µm^2, Dmca1D -RNAi, 1642 ± 236 µm^2). **C** AZ density is calculated by dividing #AZ/surface area and shows no significant difference between Dmca1D knockdown and control (mean ± SD: control, 0.35 ± 0.04 µm^{-2}; Dmca1D -RNAi, 0.33 ± 0.04). **D** Immunofluorescence of postsynaptic glutamate receptors (GluR) is not altered upon Dmca1D knockdown (blue) as compared to control (black). **E-F** Confocal Z-projections of type Ib synaptic boutons on muscle4 from control (E) and Dmca1D-RNAi (F) animals, stained for GluRIIc, Brp and Hrp. AZ densities for the selected examples are listed in Ei and Fi

Furthermore, it has previously been demonstrated that calcium influx through Dmca1D channel can be acutely reduced by the application of the biogenic amine Tyramine (Schützler et al., 2019). To acutely reduce presynaptic Dmca1D function, we bath applied 10^{-5} M of Tyramine to our preparation and measured Gcamp6m fluorescence before, during and after application of Tyramine (Fig. 5). Bath application of the

neuromodulator Tyramine significantly reduces calcium influx into the presynaptic terminal upon AP stimulation in controls but not in Dmca1D RNAi. This effect can be reversed by a 2min washout with normal saline (Fig. 5A-B). This reduction in calcium influx has no effect on evoked synaptic transmission (Fig. 5C).

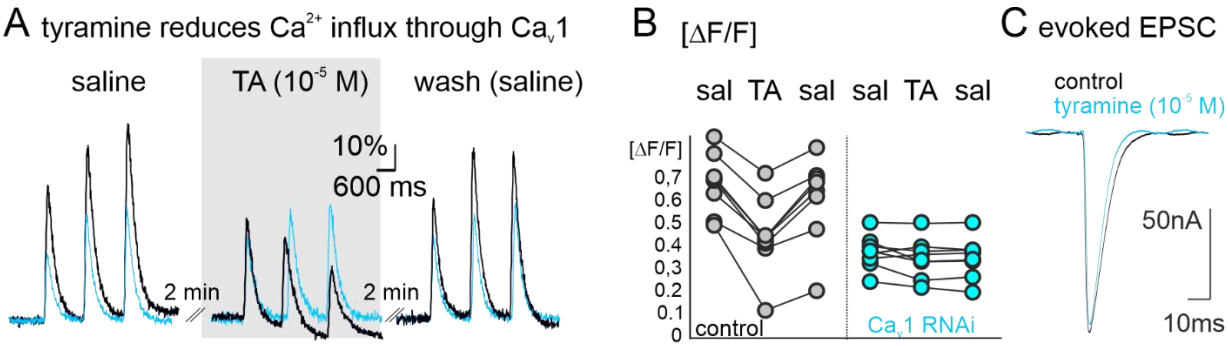

Figure 5: **Acute manipulation of presynaptic calcium influx. A** Representative traces of control and Dmca1D knockdown before, during and after the application of 10^{-5}M Tyramine. Tyramine reversibly reduces calcium influx into presynaptic terminals, but has no effect in a Dmca1D knockdown. This is quantified in **B**. **C** Application of Tyramine has no effect on SP transmission despite reducing calcium influx significantly.

3.3 Dmca1A is essential for synaptic transmission, Dmca1D fine tunes it

To analyze the function of the Dmca1D channel, we performed muscle recordings in current and voltage clamp mode from larval crawling muscles M6/7 in abdominal segments A2&A3. Despite the significant reduction of calcium influx upon acute blockage of the Dmca1D channel, it has no significant effect on synaptic transmission (Fig. 5C). We next tested the effects of genetic Dmca1D knockdown on synaptic transmission (Fig. 6). Current clamp recordings in Dmca1D knockdown and in control show no difference (Fig. 6A). Two electrode voltage clamp recordings reveal a small but significant difference in single pulse amplitude (Fig. 6B&C) and a highly significant difference in paired pulse fascilitation (Fig. 6B&D) and thus short-term plasticity.

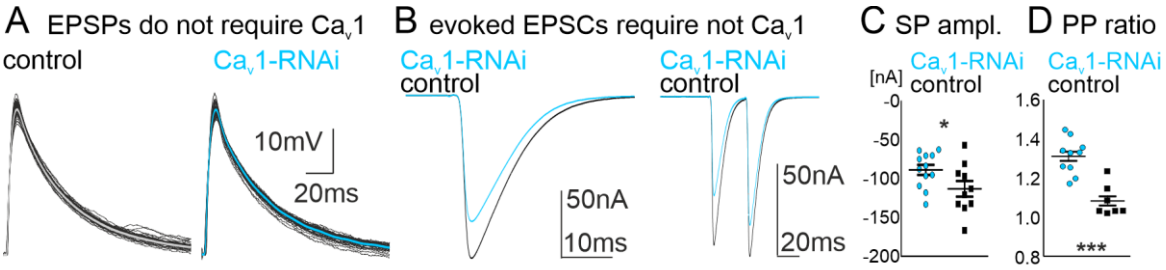

Figure 6: **Contribution of Dmca1D to synaptic transmission and short term plasticity. A** RNAi knockdown of Dmca1D shows no difference in evoked single pulse EPSPs at larval crawling muscles M6/7 in abdominal segment A2&A3. **B** Two electrode voltage clamp recordings of the Dmca1D knockdown show a minor but significant reduction in evoked single pulse EPSCs and a strong increase in paired pulse fascilitation. **C** shows the quantification of single pulse amplitude and **D** the quantification of paired pulse ratios.

To further analyze the contribution of the Dmca1D channel to synaptic transmission, we repeated the voltage clamp experiments with an external calcium concentration of 2mM instead of 0.5mM. The main difference of these two calcium concentrations is that in low calcium concentrations we expect paired pulse fascilitation at a 30ms inter pulse interval (IPI) due to residual calcium in the active zones (Nanou and Catterall, 2018), whereas in 2mM external calcium, we expect paired pulse depression due to the depletion of SVs as caused by higher mean quantal content (Nanou and Catterall, 2018). Single pulse amplitude in 2mM calcium still tends to be slightly smaller in Dmca1D knockdowns compared to control, but the effect is not significant anymore (Fig. 7A&B). Paired pulse ratio in controls show a depression as we would expect in 2mM calcium, but Dmca1D knockdowns still show paired pulse fascilitation (Fig. 7C&D). This again shows that the Dmca1D channel has only a minor function in single action potential induced synaptic vesicle release, but it alters short-term plasticity.

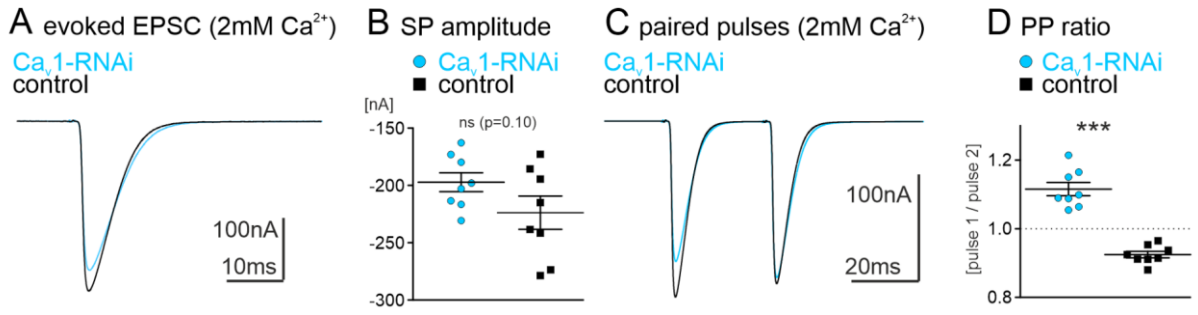

Figure 7: **Contribution of Dmca1D to synaptic transmission and short term plasticity at 2mM external Ca^{2+}. A** Traces of TEVC recordings from Dmca1D RNAi (blue) and control (black) show, that the single evoked EPSC amplitudes still tend to be smaller in Dmca1D knockdowns, but quantification shows no significant difference **(B)**. **C** Paired pulse traces show also in 2mM Ca^{2+} a fascilitation in Dmca1D RNAi whereas controls show paired pulse depression. **D** Quantification of paired pulse ratios shows a highly significant difference between Dmca1D knockdown and control.

To show that the Dmca1A and not the Dmca1D channel is required for synaptic transmission, we used the temperature sensitive mutant cac^{NT27} (Rieckhof et al., 2003) to block calcium influx mediated by Dmca1A (Fig. 8A). At non-permissive temperatures, cac^{NT27} mutants show no synaptic transmission, but synaptic transmission amplitude is normal (Fig. 8A, left). Control animals show a reduction of synaptic transmission at 35°C, but transmission still functions reliably at non-permissive temperature for the temperature sensitive Dmca1A mutant (Fig. 8A, right). Additionally, we used the FlpStop technique(Fisher et al., 2017) to knockout Dmca1A in single motoneurons and recorded from the corresponding muscle (Fig. 8B-D). Two electrode voltage clamp recordings from M12 in A2/3 show an over 90% reduction in evoked EPSC currents in flipped motoneurons compared to unflipped ones. Paired

pulse ratio in flipped and unflipped MNs shows no significant difference despite the strong reduction of current amplitude in Dmca1A knockout MNs. This shows that the Dmca1A channel is essential for synaptic transmission.

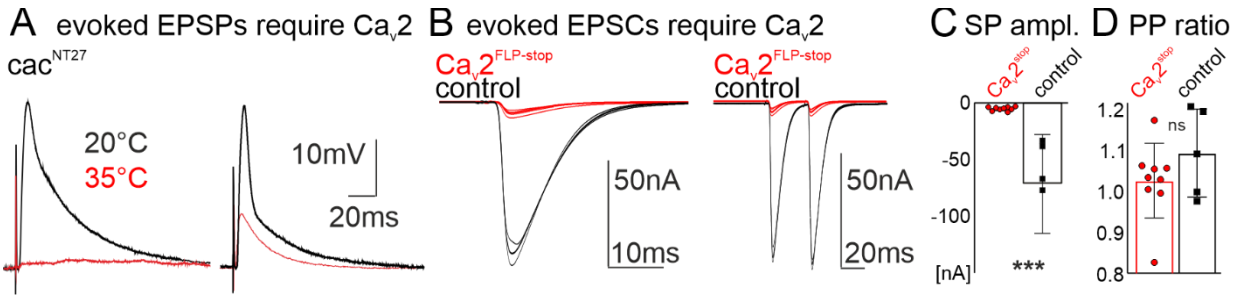

Figure 8: **Dmca1A is required for synaptic transmission. A** the temperature sensitive mutant cac^{NT27} shows no synaptic transmission at 35°C whereas control show reduced but reliable transmission. **B** Dmca1A knockout MN projecting onto M12 in A2&3 do show a strong reduction in single pulse amplitude (quantification in **C**) but maintain normal paired pulse fascilitation compared to controls (quantification in **D**).

3.4 Synaptic vesicle endocytosis is augmented by Dmca1D

Although Dmca1D localizes to presynaptic terminals of *Drosophila* larval crawling motoneurons and mediates 50% of AP induced calcium presynaptic calcium signals, synaptic transmission can be reliably induced without the presence of the Dmca1D channel. Its localization outside the active zone, kinetics (Kadas et al., 2017) and its feeding state dependent modulation by tyramine (Schützler et al., 2019) make it a prime candidate to influence activity dependent synaptic vesicle (SV) endocytosis. Synapses have to function over wide ranges of activity patterns. To do so, their exo- and endocytosis rates must be dynamically adjusted to different activity demands. Activity dependent calcium influx has been discussed over decades to fulfill this function. This idea is complicated by the fact that SV exo-and endocytosis largely occur specially separated, have different time constants and depend on different calcium concentrations (Haucke et al., 2011; Kononenko and Haucke, 2015; Maritzen and Haucke, 2017; Soykan et al., 2016, 2017). Furthermore, reliable coding of synaptic transmission likely requires independent calcium signals for exo- and endocytosis. At the *Drosophila* NMJ, separate control of synaptic vesicle exo-and endocytosis by calcium influx through distinct routes has already been discussed (Kuromi et al., 2004, 2010), but the channel responsible for endocytosis augmentation at the presynapse remained unknown. Related to the findings of Kuromi et al. 2004 & 2010, a vesicle associated calcium channel, named flower, was suggested to be responsible for the regulation of SV endocytosis (Yao et al., 2009, 2017). Although the authors claim that the newly discovered protein is conserved over all animals, the role of flower in endocytosis regulation has not been reproduced in any other system, or by others at the Drosophila NMJ. We tested the role of the Dmca1D channel in synaptic vesicle endocytosis regulation. Sustained firing at 1Hz for 60 seconds shows an increased synaptic depression upon Dmca1D knockdown in motoneurons, both in 0.5 and in 2mM external calcium (Fig. 9A-D). This hints at a contribution of Dmca1D to vesicle endocytosis. It also shows that synaptic vesicle endocytosis is not abolished, but the steady state amplitude of transmission is significantly reduced by presynaptic Dmca1D knockdown. Direct measure of vesicle uptake into presynaptic terminals, via FM1-43 imaging, further reinforces these findings, as vesicle uptake in Dmca1D knockdowns is reduced but not eliminated compared to control, while vesicle release is unaffected (Fig. 9E-G).

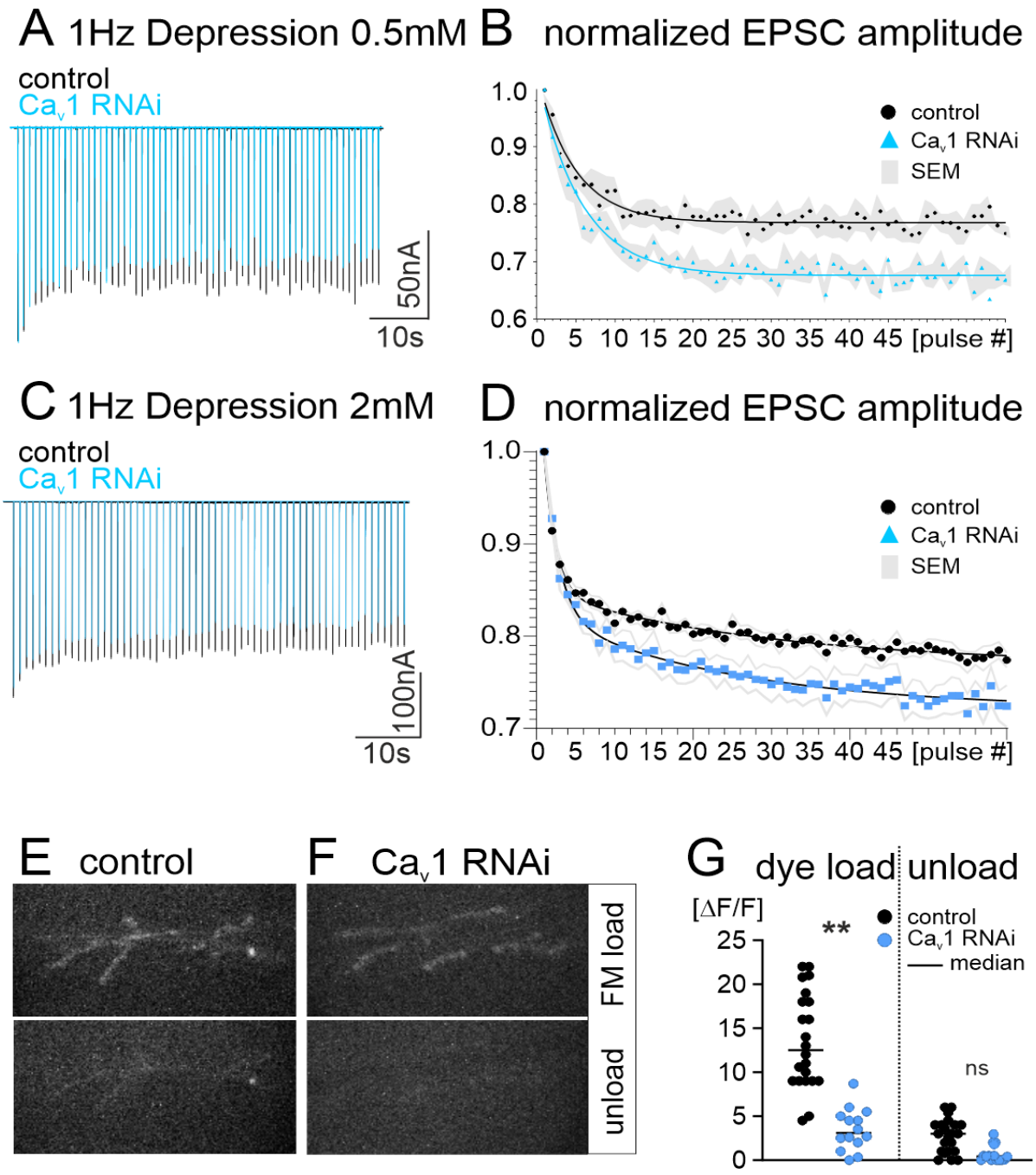

Figure 9: **Synaptic vesicle endocytosis is augmented by activity dependent calcium influx through Dmca1D.** **A** Representative recordings of PSCs from muscle M6/7 during 1 min of motoneuron stimulation at 1 Hz in control (black trace) and following Ca_v1 RNAi in motoneurons (blue trace) indicate increased synaptic depression with Ca_v1 RNAi. **B** For quantification PSC amplitude was normalized to the first PSC and averaged over 9 control animals (black circles) and 12 Cav1 knock down animals (blue triangles). Curves for fitted with (one term exponential standard fit by Chebyshev). Grey shaded areas represent the standard error of the mean (SEM). Steady state synaptic depression is reached after ~25 stimuli and 10% increased by Ca_v1 RNAi. **C** In 2 mM external Ca^{2+}, PSC depression during 1Hz motoneuron stimulation is increased by Ca_v1-kd in motoneurons (blue trace) as compared to control (black trace). **D** PSC amplitude normalized to the first PSC and averaged over 8 control (black circles) and 8 Ca_v1-kd animals (blue squares). Lines represent single exponential fits and grey areas the SEM. After 35s near steady state synaptic depression at 0.78 of the initial amplitude is reached. Ca_v1-kd increases synaptic depression by ~25% to 0.72 in steady state. **E-F** Upper panels (FM load) show representative images of FM1-43 dye taken up into recycled synaptic vesicles in motor terminals on M6/7 by stimulation with high K^+ (20mM) for 3 minutes followed by 3 minutes wash in Ca^{2+} free saline in a control (left) and with Ca_v1 RNAi (right). Lower panels (unload) show nearly complete unloading of labeled SV by re-stimulation for 5 minutes in high K^+ and washing for 3 minutes in zero Ca^{2+} saline in control (left) and with Ca_v1 RNAi (right). **G** Quantification of fluorescence changes as caused by FM loading and unloading reveals significantly reduced synaptic vesicle recycling (dye load) with Ca_v1 knock down (blue circles) as compared to control (black circles). By contrast, activity induced synaptic vesicle release (unload) is not significantly affected.

3.5 The membrane bound calcium ATPase PMCA localizes to the periactive zone of presynaptic terminals

We identified two different calcium channels at the presynaptic membrane, whose calcium signals are used for two different, fundamentally important synaptic functions, exo- and endocytosis. These channels are spatially separated from each other; Dmca1A localizes to active zones, but Dmca1D localizes outside active zones. The functional coupling between calcium channels and SVs decreases with the decreasing calcium concentrations during diffusion with the square of distance (Eggermann et al., 2013). Therefore, the Dmca1A channel in the AZ would be defined as a tightly coupled channel, whereas the Dmca1D channel in periactive zone would be a loosely coupled channel for SV exocytosis. This can already be deduced from the TEVC recordings, which show elimination of synaptic transmission upon Dmca1A block, and only a small reduction in single pulse amplitude in low calcium concentrations upon Dmca1D knockdown along with Dmca1Ds more significant functions in short-term plasticity and SV endocytosis. The calcium micro- and/or nanodomains generated by Dmca1A are restricted in space and time by calcium binding proteins in the active zone and soluble buffers (Eggermann et al., 2013). Consequently, remaining cytosolic Ca^{2+} in the presynaptic terminal after nanodomain collapse is reduced by diffusion and buffering to nanomolar concentrations (Delvendahl et al., 2015). This ensures the temporal precision of excitation-release coupling and repeated release during sustained activity (Delvendahl et al., 2015). In contrast to the extensive knowledge of calcium handling during nanodomain collapse, the reverse scenario has not been thoroughly addressed, i.e. it remains largely unknown whether and how calcium nanodomains are protected from other calcium signals in the presynaptic terminal. We hypothesize the existence of such a mechanism because it seems essential to ensure stable mean quantal content, and thus coding reliability, independent of physiological calcium signals directly adjacent to active zones. Given that the calcium concentrations that are necessary to accelerate SV endocytosis are in the micromolar range (Leitz and Kavalali, 2015; Thomas et al., 1994), we predict an effective mechanisms for functional separation of calcium influx through Dmca1A in active zones and Dmca1D in periactive zones. In addition to the previously known mechanisms of presynaptic calcium buffering, we now find a plasma membrane bound calcium ATPase (PMCA), localizing outside the active zone of *Drosophila* crawling motoneurons (Fig. 10A-C).

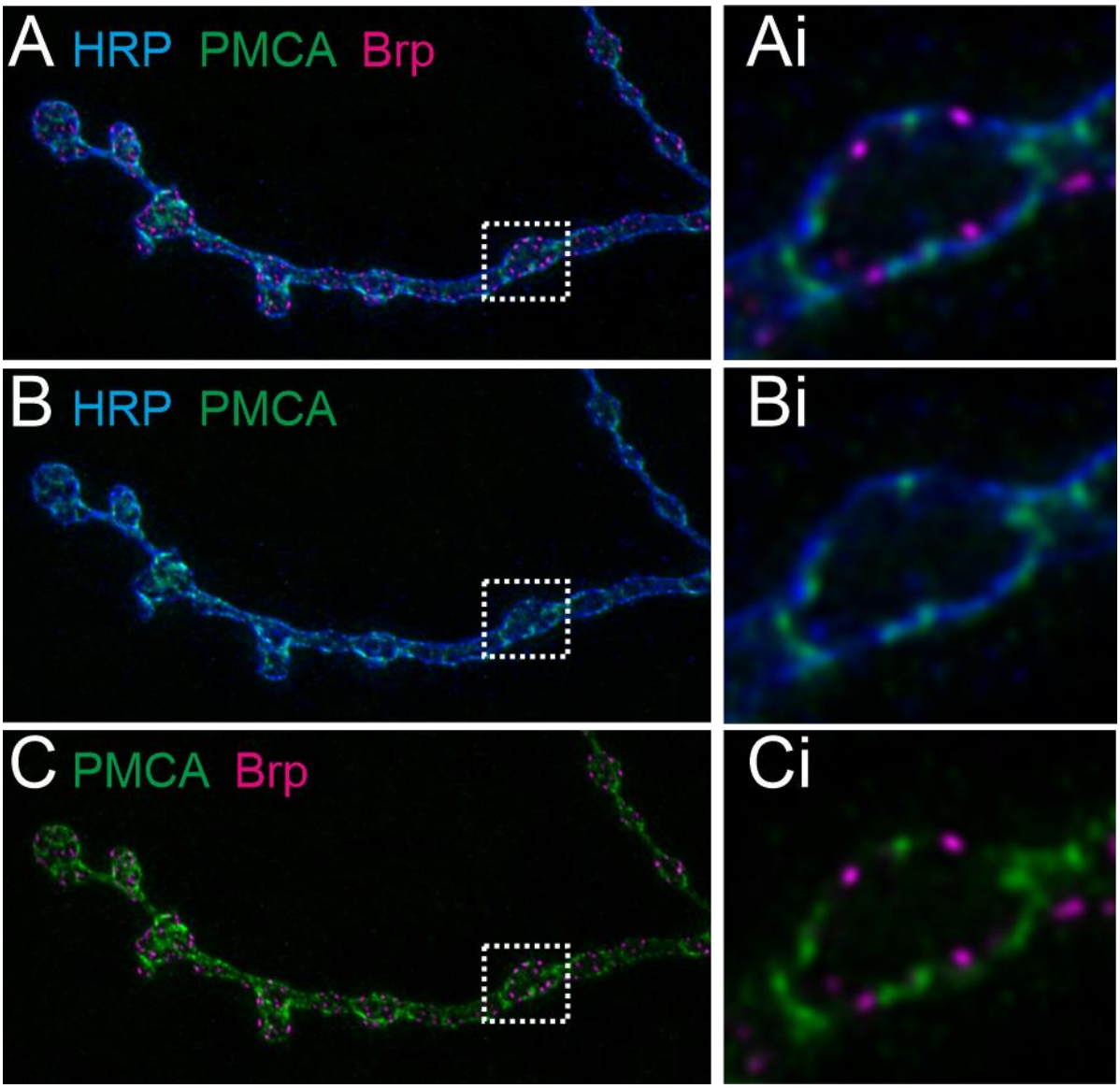

Figure 10: **Presynaptic localization of PMCA. A-C** representative triple label of presyanptic terminals with *α*-HRP (blue) to stain the plasma membrane, α-BRP (magenta) as an active zone marker and GFP tagged PMCA (green). **Ai-Ci** enlarged single slices, marked as dotted squares in A-C.

PMCA has already been described at vertebrate (Schmidt et al., 2017) and invertebrate presynaptic terminals (Lnenicka et al., 2006), but its precise localization and function was not sufficiently investigated. To determine its precise presynaptic localization, we used a GFP tagged PMCA. Since the PMCA is also present in the muscle and highly enriched in the subsynaptic reticulum (SSR) (Fig. 11A), we drove expression of postsynaptic GFP RNAi in muscles to eliminate background staining (Fig. 11B). To further reduce backround staining from the SSR, we combined the GFP RNAi with deGradFP (Caussinus et al., 2012), a GFP-specific nanobody, which targets endogenously tagged PMCA for degradation and reveals the precise subcellular localization of presynaptic PMCA outside active zones (Fig. 10A-C, 11C). We cross-validated the presynaptic PMCA localization and knockdown efficiency by presynaptic

PMCA-RNAi at larval NMJs which were outlined with Hrp (Fig. 11D&E). Postsynaptic knockdown of PMCA shows PMCA-specific patches along presynaptic terminals with weak background staining from the SSR (Fig. 11Di) while concomitant pre-and postsynaptic PMCA knockdown strongly reduces PMCA immunostaining (Fig. 11Ei). Remaining signal can be visualized by using 3-fold-intensity (Fig. 11Ei inset) and displays knockdown efficiency of the presynaptic PMCA knockdown.

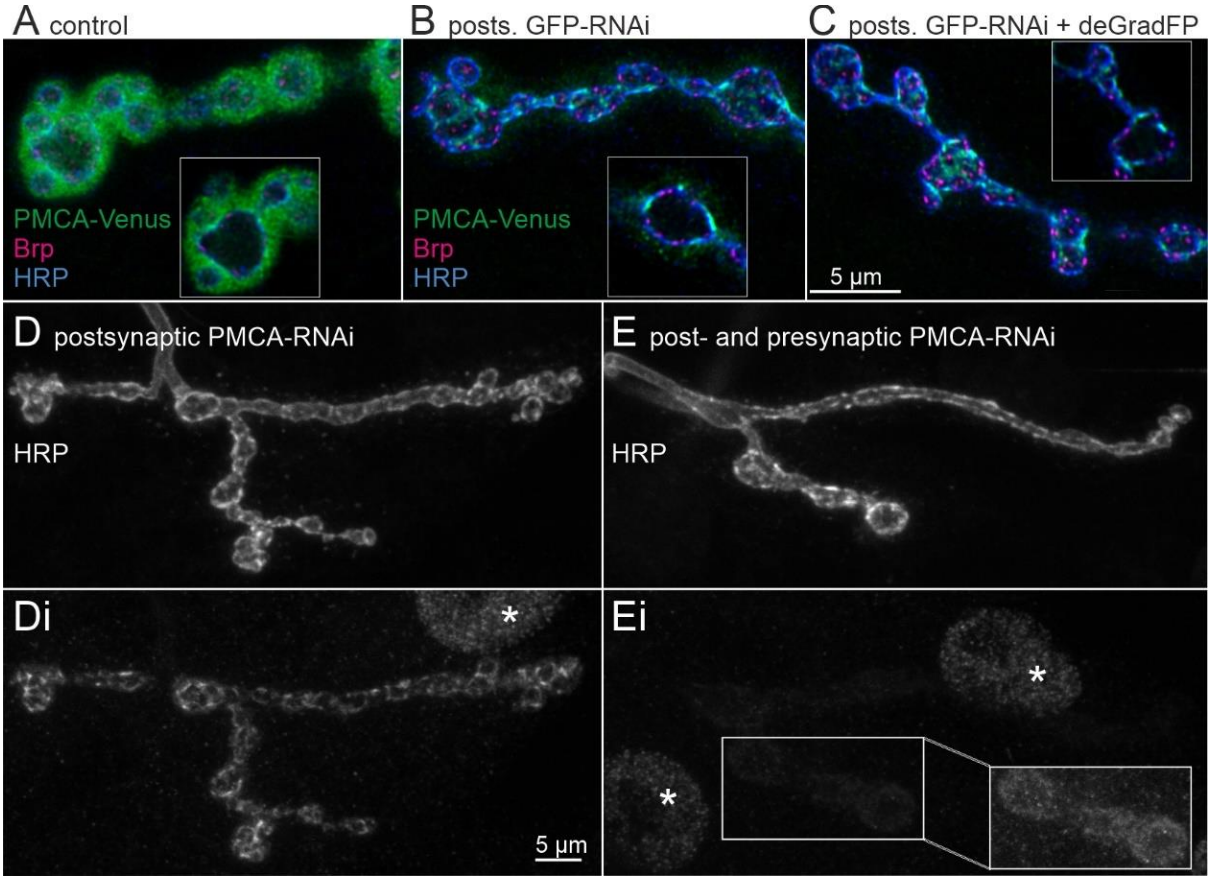

Figure 11: **Disclosure of PMCA localization at periactive zones of motoneuron terminals. A-C** Confocal Z-projections of type Ib synaptic boutons on muscle 4, decorated with genomically Venus-tagged PMCA (green) and labeled for the AZ marker Brp (magenta) and the neuronal surface marker Hrp (blue). **A** In controls (C57-Gal4/+; PMCA[CPTI001995]/+), PMCA is enriched in the subsynaptic reticulum (SSR), a convoluted specialization of the synaptic sarcolemma. Bright signal from PMCA-Venus in the SSR hinders optical separation from potentially presynaptically localized PMCA-Venus. This problem persists at the level of single optical sections (inset). **B** Postsynaptic, i.e. muscle-specific GFP-RNAi (C57-Gal4/UAS-GFP-RNAi; PMCA[CPTI001995]/+) reduces SSR-associated PMCA-Venus such that Venus signals along the Hrp-labeled membrane become visible. **C** This effect is sharpened, if concomitant with GFP-RNAi, deGradFP is co-expressed to target PMCA-Venus for degradation by a GFP-specific nanobody fused to ubiquitin ligase (+/UAS-Nslmb-vhhGFP4; C57-Ga4/UAS-GFP-RNAi; PMCA[CPTI001995]). **D-E** Cross-validation of presynaptic PMCA localization and its efficient knockdown by PMCA-RNAi at NMJs on muscle 4, outlined by Hrp-labeling. **D** Postsynaptic PMCA-RNAi (+/UAS-PMCA-RNAi; C57-Gal4/+) uncovers PMCA-specific patches of immunofluorescence along boutons, surrounded by weak SSR labeling (Di). **E** Combined pre- and postsynaptic PMCA-RNAi (OK371-Gal4/UAS-PMCA-RNAi; C57-Gal4/+) reveals the efficiency of the motoneuronal knockdown (Ei). The boxed set of boutons is shown at 3-fold intensity to show some remaining signal. Asterisks mark unspecific labeling of nuclei by the pan-PMCA antibody.

3.6 PMCA functionally isolates Dmca1A and Dmca1D calcium signaling

To test the potential function of PMCA in separating presynaptic calcium signals mediated via Dmca1A and Dmca1D, we used a presynaptic PMCA RNAi and measured evoked ePSCs in TEVC. Following PMCA knockdown, ePSCs are significantly increased compared to controls (Fig. 12A, B & D). Quantification shows that current amplitude, area, and decay τ are significantly increased, whereas rise τ is unaffected (Fig. 12E-H). Also, paired pulse ratio is shifted from fascilitation in controls to depression in PMCA knockdowns due to increased first pulse amplitude (Fig. 12I, J). Co-expressing a Dmca1D knockdown together with the PMCA knockdown fully rescues the phenotypes caused by PMCA knockdown alone, except paired pulse ratio, which is only rescued partially (Fig. 12 A-J). These findings provide evidence that presynaptic PMCA functions not only as a Ca^{2+} extruder to keep calcium levels at a nontoxic level (Lnenicka et al., 2006), but its strategic subcellular localization surrounding active zones indicates its function in protecting the active zone from external calcium sources.

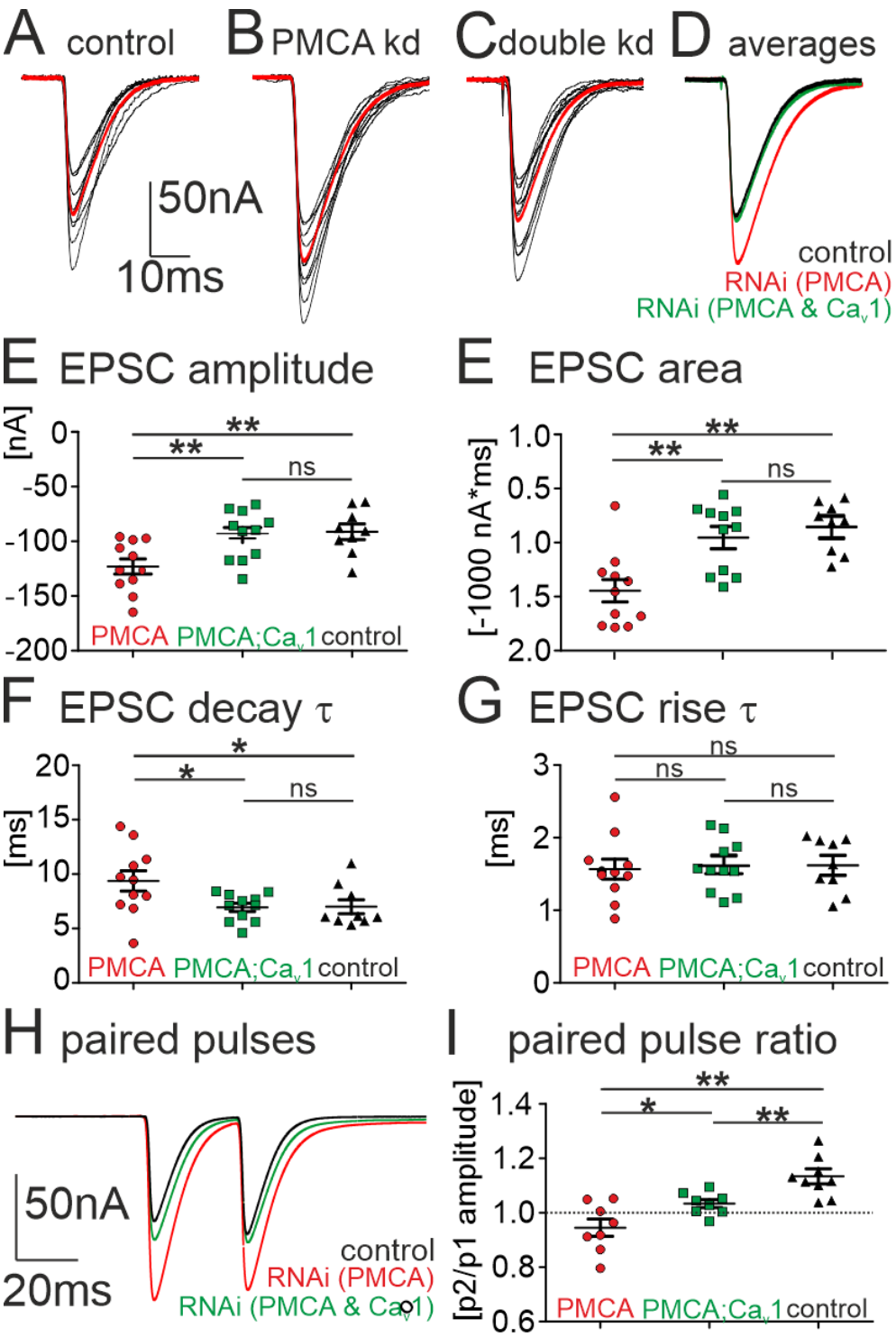

Figure 12: **Presynaptic PMCA RNAi increases evoked ePSC and is rescued by concomitant Dmca1D knockdown. A-D** Evoked PSCs from muscle M6/7 as multiple sweeps (black traces) and average (red) in a representative control (A), following PMCA RNAi knock down in motoneurons (B), and following PMCA and Dmca1D double knock down (C). **D** Overlay of averages shows increased amplitude in PMCA knock down (red) versus control (black), and rescue by PMCA, Dmca1D double knock down (green). Quantification shows significant increases of PSC amplitude (**E**), area (**F**), and time constant of decay (**G**) by presynaptic PMCA knock down (red circles) as compared to control (black triangles). Effects of PMCA knock down on evoked synaptic transmission are rescued by concomitant Dmca1D channel knock down (green squares). **H** PSC rise time is not affected by PMCA knock down or PMCA, Dmca1D double knock down. **I** Paired pulse fascilitation in controls (black) is reversed to paired pulse depression upon PMCA RNAi (red). Concomitant Dmca1D knock known partially rescue rescues paired pulse ratio (green).

To directly measure calcium influx into the AZ, we used Gcamp6s coupled to the bruchpilot protein(Kiragasi et al., 2017) and evoked 10 action potentials at a frequency of 100Hz. Using this stimulation paradigm, we made sure to evenly excite all AZs. Consistent with our previous findings, PMCA knockdown significantly increases calcium influx into AZs, whereas Dmca1D knockdown alone has no effect on AZ calcium signals (Fig. 13A-C).

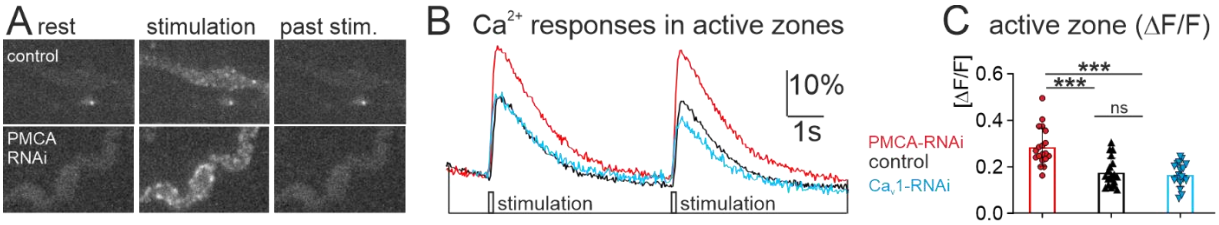

Figure 13: **Increased Ca^{2+} influx into AZ zones upon PMCA knockdown. A** Representative pictures of presynaptic terminals with with Gcamp6s coupled to brp in control and PMCA RNAi at rest, during stimulation (10AP at 100Hz) and after stimulation. **B** Traces of ΔF/F for two stimulations in Control (black) PMCA RNAi (red) and Dmca1D RNAi (Blue), showing a significant increase in calcium inlflux into AZ upon PMCA knockdown, while Dmca1D knockdown alone has no effect. **C** quantification reveals an almost doubled calcium influx into AZ upon PMCA knockdown.

Ultimately, with use of the calcium chelator EGTA-AM, which has slow Ca^{2+} binding kinetics (Genç and Davis, 2019) and prevents the recruitment of loosely coupled vesicles for fusion (Genç et al., 2017; Schneggenburger and Neher, 2005), we could further substantiate the acute function of PMCA in protecting the AZ. Increased single pulse current amplitude in PMCA knockdown is rescued by application of membrane permeable EGTA to control amplitude, whereas decay τ is still increased (Fig. 14A-C).

The increased decay τ could have various explanations. It could either be caused by calcium induced calcium release from internal calcium stores in the presynaptic terminal or by developmental defects in the pre-and/or in the postsynapse on the level of protein composition, but we did not test for this during the time course of this thesis but we did test developmental defects on the structural level (see below).

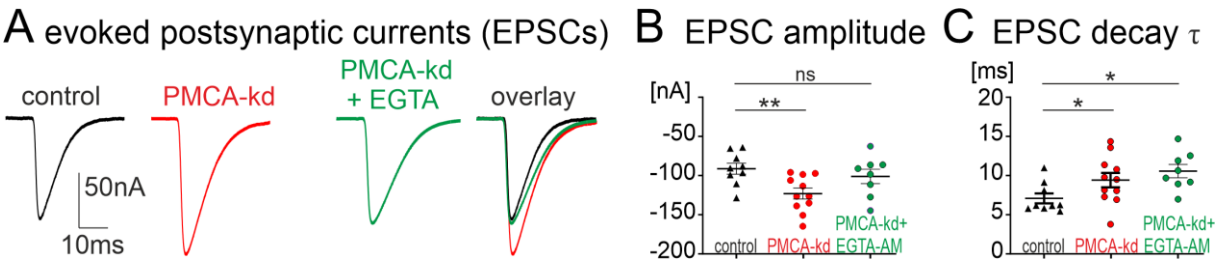

Figure 14: **Increased synaptic transmission upon PMCA knockdown is rescued by application of EGTA. A** Avereages of postsynaptic currents for control (black), PMCA RNAi (red) and PMCA RNAi + 25µM EGTA-AM (green). Increased synaptic transmission caused by PMCA RNAi can be fully rescued by 10min incubation of EGTA-AM in calcium free saline, followed by 3 times washing with normal HL3.1 Saline (0.5mM Ca^{2+}) with quantification in **B.** The overlay already shows a still increased decay τ after EGTA-AM incubation which we quantified in **C.**

To address the functional relevance of the PMCA knockdown, we analyzed larval body size and crawling speed. PMCA knockdown increases muscle tone, resulting in a 25% reduction of larval body length, which can also be rescued with a concurrent Dmca1D knockdown (Fig. 15A, B). During crawling, increased synaptic transmission causes spasms/cramps, which lead to significantly decreased crawling speed (Fig. 15C). The deficits in crawling speed are partially rescued by the double knockdown of PMCA and Dmca1D. Dmca1D RNAi alone has no effect on crawling speed (Fig. 15C).

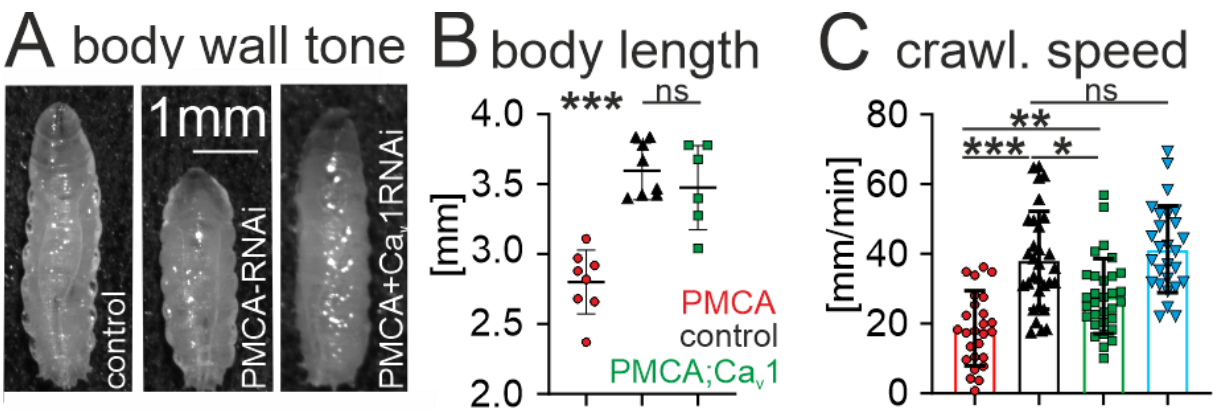

Figure 15: **Functional conesquences of PMCA RNAi. A** PMCA knockdown larvae display an increased muscle tone, resulting in significant body length shortening. Concomittant Dmca1D knockdown rescues body length as quantification shows **(B). C** crawling speed in PMCA RNAi (red circles) is significantly reduced compared to control (black triangles) and is parially rescued by PMCA and Dmca1D double knockdown (green squares). Dmca1D knockdwon (blue triangles) alone has no effect on crawling speed

In order to exclude developmental defects in synaptic structure causing the observed increases in synaptic transmission by PMCA knockdown, we analyzed the number of active zones, bouton size and calculated AZ density for PMCA knockdown, PMCA and Dmca1D double knockdown as well as controls. PMCA knockdown causes a significant reduction in the number of AZs as compared to control (Fig. 16A) along with a significant increase in bouton surface (Fig. 16B, Ei, Fi), resulting in a highly significant reduction of AZ density (Fig. 16C, Eii, Fii). These phenotypes are rescued by concomitant knockdown of the Dmca1D channel (Fig. 16A-C, Gi, Gii). However, decreased active zones and hence active zone density should result in decreased synaptic transmission, but the opposite is the case. Therefore, it seems unlikely that developmental effects of PMCA knockdown on presynaptic structure cause the resulting physiological phenotype. On the postsynaptic site, the normalized intensity of glutamate receptor immunostaining is significantly increased upon PMCA knockdown compared to controls and is rescued by a concomitant knockdown of the Dmca1D channel (Fig. 16D-G). Reducing the number of AZ at the presynapse and

simultaneously increasing postsynaptic receptors are mechanisms of homeostatic compensation that should ultimately result in a normal phenotype of synaptic transmission. Hence, we conclude that besides effects of presynaptic PMCA knockdown on presynaptic structure, and compensatory effects on the postsynaptic side, the amplitude of synaptic transmission is significantly increased in PMCA knockdown because of the loss of AZ protection from calcium influx through Dmca1D channels. This interpretation is supported by our finding of acute rescue of synaptic transmission amplitudes as resulting from PMCA knockdown by EGTA. EGTA competes with the contribution of loosely coupled calcium channels to SV release, and this restores normal synaptic transmission amplitudes in the presence of developmental effects on presynaptic structure and postsynaptic receptor expression.

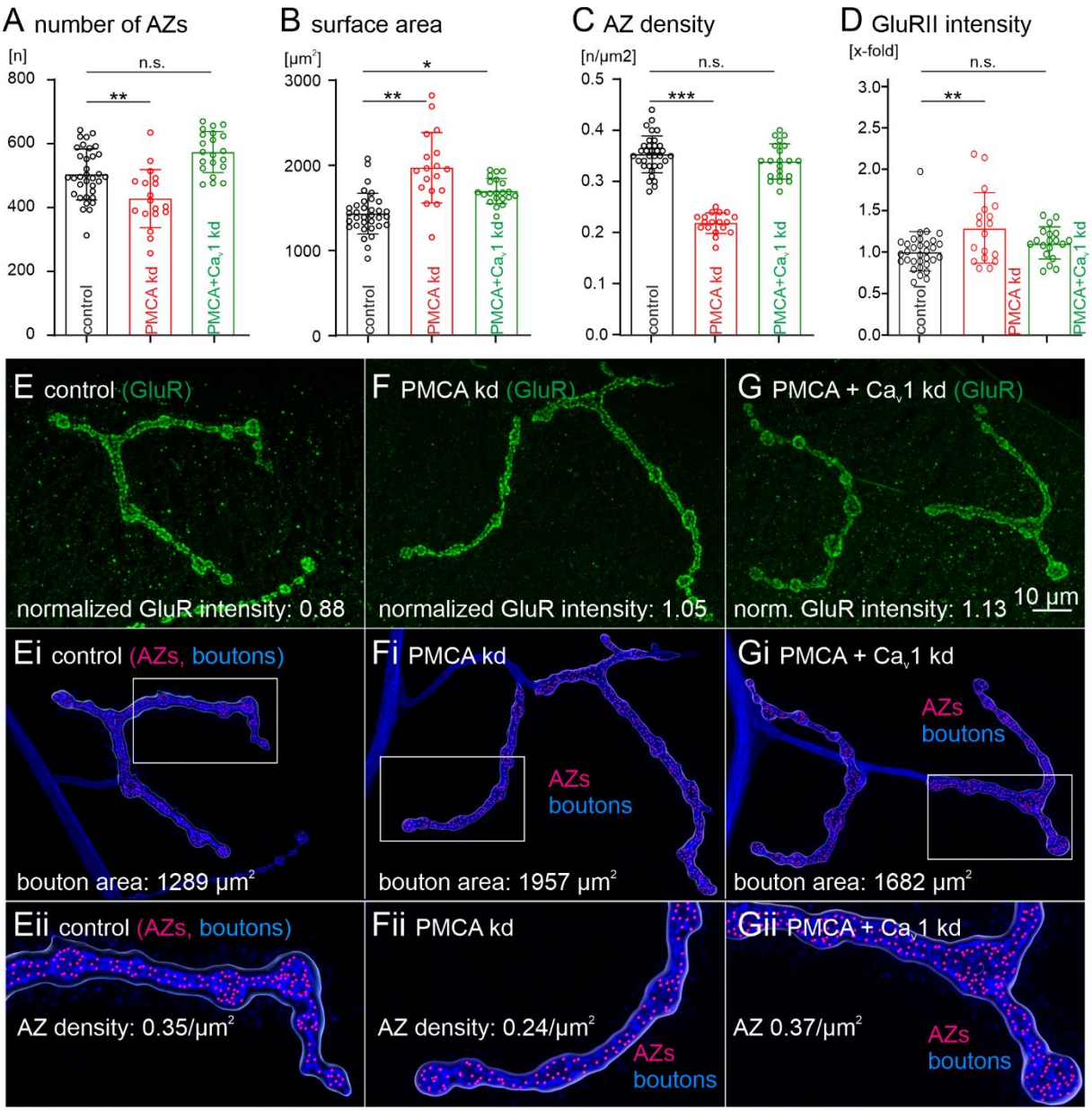

Figure 16: **Effects on bouton morphology by PMCA RNAi and PMCA&Dmca1D double RNAi. A** PMCA RNAi decreases the number of AZ of presynaptic terminals on muscle M4 in segments A2 and A3 significantly compared to control (black). AZ number is rescued by PMCA&Dmca1D doubleknockdown (green). **B** Additionally to the decreased number of AZ, the overall bouton surface is increased in PMCA knockdown (red) compared to control (black) and rescued by double knockdown of PMCA and Dmca1D (green). **C** decreased AZ number and increased bouton size result in significantly decreased AZ density in PMCA RNAi (red) but are similar in control (black) and PMCA & Dmca1D doubleknockdown (green). **D** postsynaptic immonulabeling of GluRs shows a signficiant increase in PMCA knockdown compared to control and rescued upon concomittand Dmca1D knockdown. **E-G** Images of example NMJs from the analysis shown in A-D. Upper row shows GluRIIc-specific immunolabeling of entire NMJs from control (E), PMCA-kd (F) and PMCA-Dmca1D double knockdown larvae (G). The overall GluR intensity normalized to the mean of controls is provided for each example. Middle row (Ei-Gi) displays the same NMJs after defining bouton areas as 3D ROIs (light blue outline) based on Hrp-labeling (blue) and spot detection of AZs (magenta) based on Brp-labeling. ROIs are restricted to areas containing AZs. Boxed areas are depicted as close-ups in the bottom row (Eii-Gii) with each AZ density value referring to the entire NMJ. Note that the gross morphology is similar in all genotypes. Functionally, the observed parallel increase in GluR labeling intensity and decrease in AZ number (A) and density (C) cannot explain the ~50% increase in evoked synaptic transmission by ~50% as observed with PMCA knockdown.

After investigating the function of PMCA in AP induced synaptic transmission, we analyzed its function in protecting the readily releasable pool during rest by quantifying spontaneous mini excitatory postsynaptic currents (mEPSC). Upon PMCA knockdown, TEVC recordings in TTX (10^{-5} M) show a highly significant increase in mEPSC frequency and mean amplitude (Fig. 17A-F). Concomitant knockdown of PMCA and Dmca1D partially rescues spontaneous release (Fig. 16A-F). This indicates that PMCA protects the AZ not only from calcium influx through Dmca1D, but from Ca^{2+} spillover from multiple sources. The smallest unitary events (asterisks in Fig. 16 A, B and C) are of equal amplitude in each genotype. This shows that that filling of synaptic vesicles is unaffected by PMCA RNAi (control, 0.6 ± 0.08 nA; PMCA kd, 0.68 ± 0.16 nA, p = 0.29, unpaired t test with Welch's correction). This control is important because PMCA has also been implicated in regulating the amount of neurotransmitter in SVs (Ono et al., 2019).

The increase in mean mEPSC amplitude is likely due to the high frequency of spontaneous events, resulting in fusions of multiple events (arrowheads Fig. 17B), which are very hard to discriminate. Therefore, a proper quantal analysis in TEVC for PMCA knockdown animals is complicated. In fact, quantal analysis of electrophysiologically measured spontaneous events is further complicated by the large size of the muscle fiber that is innervated by distributed axon terminals carrying roughly 500 active zones (Fig. 16 A). Depending on the distance of an active zone from the site of recording, the amplitudes, as well as the rise and decay times of mEPSCs differing, an analysis of unitary size events in electrophysiolocial experiments is error prone.

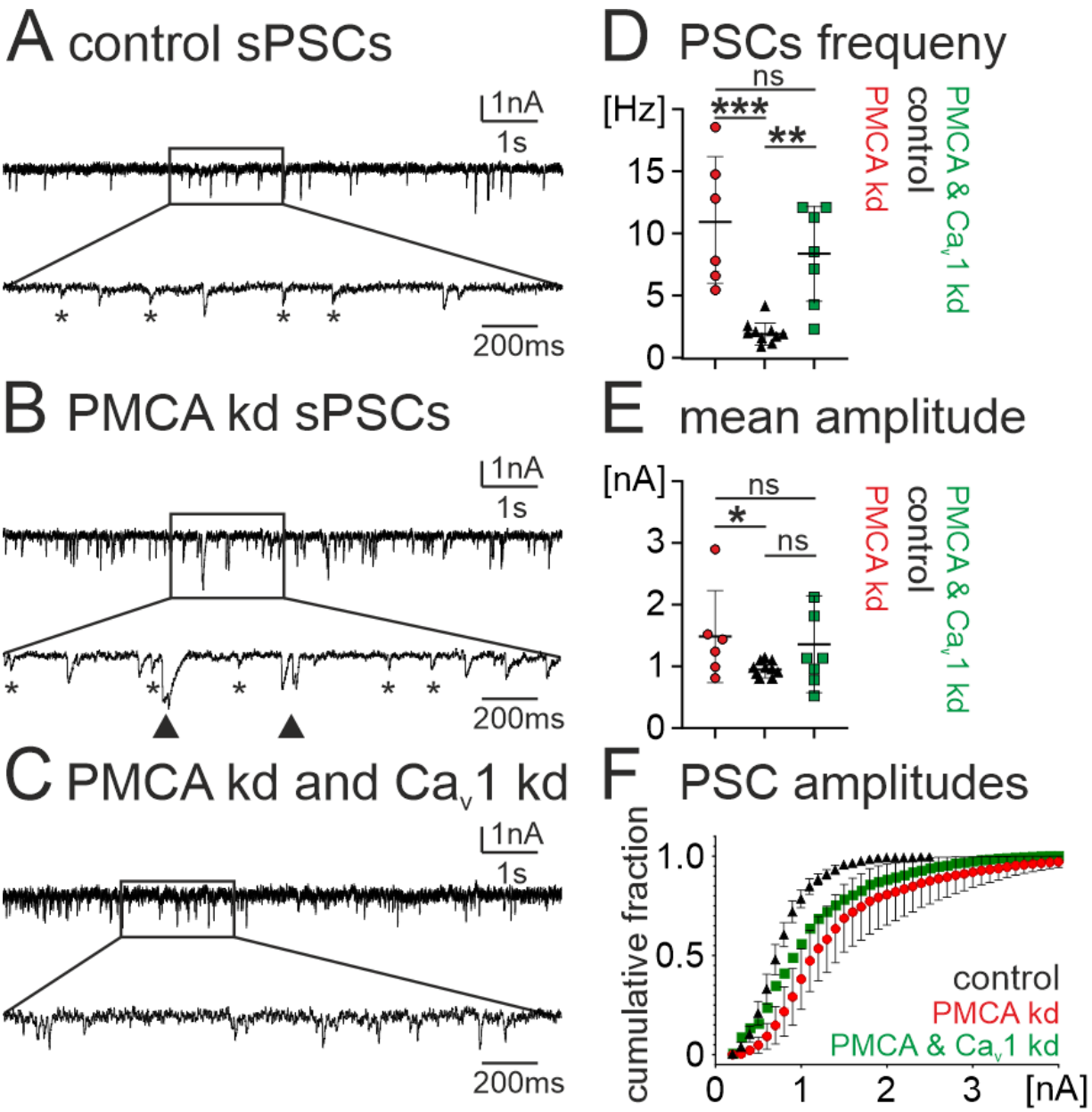

Figure 17: **PMCA controls spontaneous mEPSC from multiple sources. A-C** representative TEVC traces of spontaneous miniature excitatory postsynaptic currents in controls (A), PMCA knockdown (B) and PMCA and Dmca1D double knockdown (C) in TTX (10^{-5}M). Lower traces show the marked area in the corresponding upper trace at a larger timescale. Asterisks mark smallest unitary events which do not differ between genotypes (control, 0.6 ± 0.08 nA; PMCA kd, 0.68 ± 0.16 nA, PMCA, Cav1 kd, 0.64 ± 0.15 nA). **D** mEPSC frequency shows a highly significant increase (red dots) compared to control (black triangles) and can be partially rescued by concomitant Dmca1D knockdown (green squares). **E** Mean mEPSC frequency is increased in PMCA RNAi (red dots) compared to control (black triangles) and rescued upon concomitant knockdown of Dmca1D (green squares).**F** cumulative blotting of mEPSC shows, that in PMCA RNAi (red dots), event size starts at the same size as in controls (black triangles), but their relative percentages are very small and PMCA knockdowns show more spontaneous events of higher amplitudes, what is probably an artefact that results from the very high mEPSC frequency. This is slightly shifted back by double knockdown of PMCA and Dmca1D (green squares).

To circumvent measuring signals from all AZ projecting onto the muscles M6 and M7, as we do in TEVC, we expressed a membrane tethered Gcamp6m in the muscles of *Drosophila* larvae as a reporter for postsynaptic calcium influx through glutamate receptors in response to spontaneous vesicle release. Using this technique, we confined the area of interest to the level single receptor fields. In controls (Fig. 18 A, B),

measured spontaneous events show a quantal distribution when plotted in frequency histograms. Single events (smallest unitary amplitudes) are predominant, whereas two and threefold amplitudes occur with lower probabilities (Fig. 18B black bars). In PMCA RNAi distribution percentage of single events is strongly reduced and shifted to higher postsynaptic response amplitudes (Fig. 18C, D). This again provides evidence that PMCA keeps calcium levels in AZs in check to control release probability. Knockdown of PMCA together with Dmca1D brings quantal distribution back to control levels (Fig. 18E, F).

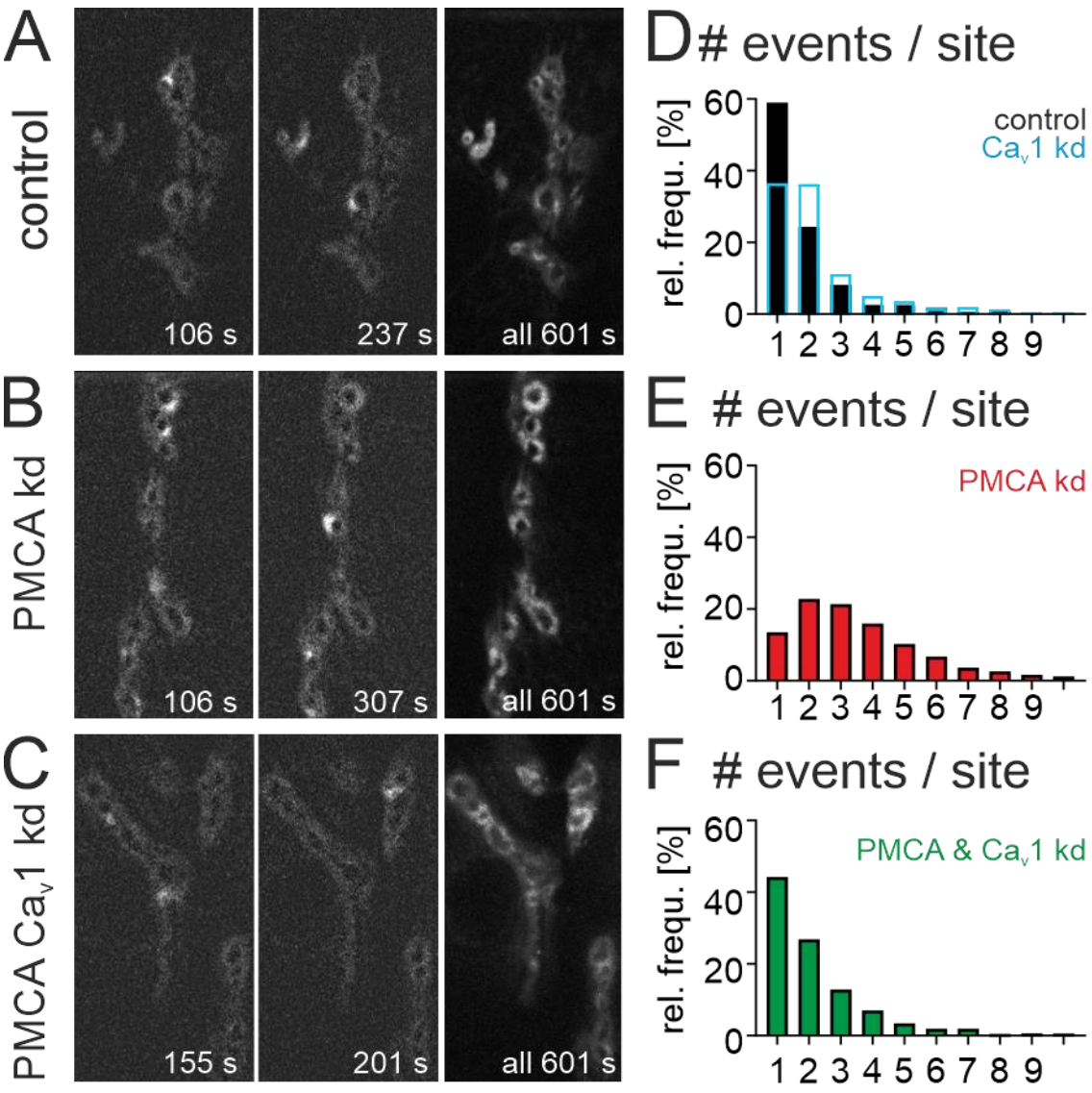

Figure 18: **Postsynaptic Ca^{2+} imaging of spontaneous release.** Representative movies of postsynaptic imaging for control **(A)**, PMCA RNAi **(C)** and PMCA and Dmca1D double knockdown **(E)**. First two frames represent a single time point during imaging, the third frame is a maximum projection over all 601 slices of imaging. Imaging was performed in 10^{-5} M TTX. **B** Frequency distribution of fluorescence intensities analyzed separately for each postsynaptic and binned to multiple integers of smallest amplitude unitary events is dominated by unitary events in controls (black bars) and not significantly affected by Cav1 RNAi in motoneurons (blue). Upon PMCA RNAi frequency distribution is shifted to higher numbers **(D)** and is rescued by concomitant knockdown of PMCA and Dmca1D **(F).**

Multiple amplitudes are unlikely caused by spontaneous multi-vesicular release from single AZ, but rather by simultaneous release from neighboring AZs. The Gcamp6m reporter is enriched in the subsynaptic reticulum around the glutamatergic receptor fields. Therefore, simultaneous release from adjacent active zones likely causes fused calcium signals from the respective opposing postsynaptic sites. This is supported by co-labeling of presynaptic AZ and recording Gcamp6m signal from the postsynapse (Fig. 19). From this we can conclude that functional coupling of neighboring active zones in the absence of PMCA significantly increases mean quantal content during evoked release and not by increased vesicle release from single AZs (Fig. 11 B&E).

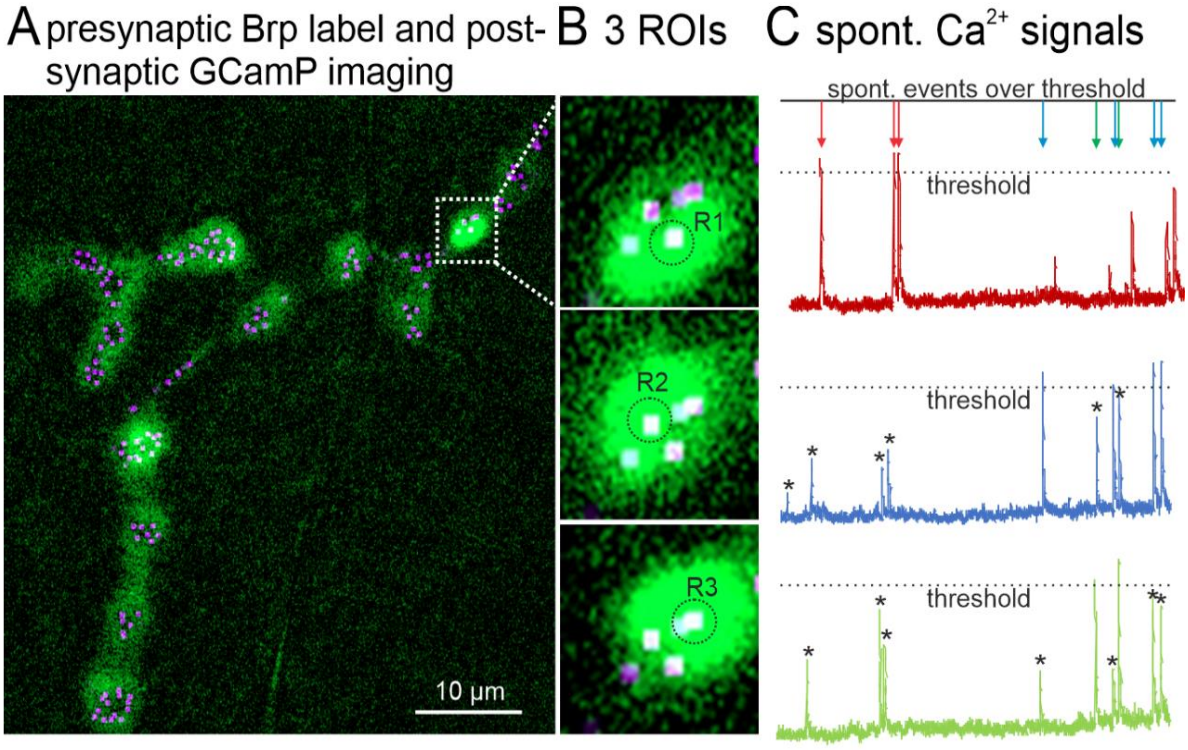

Figure 19*:* **Spontaneous release from neighboring AZ can project into the same postsynaptic receptive field. A** Overview of motorneuron axon terminals on a representative part of muscle M6/7 with Brp labeled presynaptic active zones (magenta) and a maximum projection over time of postsynaptic Ca^{2+} responses to spontaneous SV release. Dotted white square demarks bouton that is selective enlarged for 3 single time points in B. **B** At each of the three time points, one region of interest (R1-3) is positioned in the center of the postsynaptic Ca^{2+} signal. The centers of postsynaptic Ca^{2+} signals are each congruent with one presynaptic active zone (see dotted black circles), but the perimeter of each postsynaptic Ca^{2+} signal encloses multiple presynaptic active zones. Diffuseness and broadness of postsynaptic calcium signals indicate a mixed signal that is dominated by SV release from the nearest AZ but contaminated with signal caused by release from close by AZs. The membrane bound postsynaptic Ca^{2+} indicator is enriched around postsynaptic glutamate receptor fields and thus detects Ca^{2+} signals caused by SV release from multiple neighboring active zones in 3-dimensional space. **C** Plotting the postsynaptic Ca^{2+} responses for each region of interest over time reveals largest amplitude unitary signals as well as numerous signals of smaller amplitudes. This likely reflects SV release the nearest (largest unitary amplitude signals) and from adjacent or out of focus active zones (smaller amplitude signals). Thresholding (see dotted lines) allows isolation of unitary amplitude postsynaptic responses to spontaneous release of single SVs from identified active zones (see color coded arrows). Asterisks demark smaller amplitude events which are likely caused by SV release from active zones outside the center of the region of interest.

To visualize functional coupling of neighboring AZ during action potential firing, we again utilized calcium imaging of postsynaptic receptor fields and artificially evoked APs. In controls, per presynaptic AP on average 2-3 postsynaptic sites are activated underneath one presynaptic type 1b bouton (Fig. 20A, closed white circles). Upon presynaptic PMCA knock-down, the number of postsynaptic sites activated by one AP is increased (Fig. 20B, closed white circles). In particular, we observed co-activation of many neighboring sites during any given stimulus, indicating that the isolation of presynaptic AZs from Ca^{2+} spill over from their neighbors is lost, although the systems tries to compensate for that by decreasing AZ density (Fig. 16C). This co-activation of neighboring sites complicated accurate counts of active sites per stimulus. Therefore, per AP we normalized total postsynaptic fluorescence under each bouton to bouton size. PMCA knock-down causes a more than twofold increase in evoked responses imaged on the level of single boutons, and this effect is rescued by concomitant knock-down of presynaptic Ca_v1 channels (Fig. 20C, D)

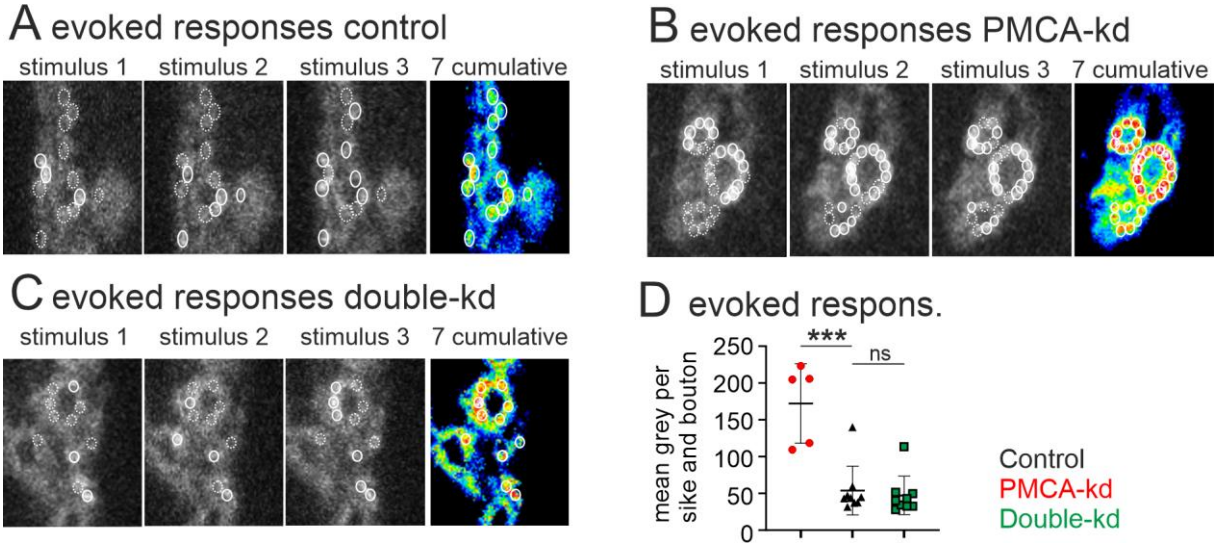

Figure 20: **Postsynaptic Ca^{2+} imaging of evoked release. A-D** postsynaptic calcium signals upon AP induced synaptic transmission for control (A) and PMCA knockdown (B). **A** In response to each presynaptic action potential (exemplified for 3, stimuli 1-3) a different subset of distinct postsynaptic sites (closed white circles) is activated underneath type 1b boutons of M6/7, while other sites remain silent (dotted white circles). The number of activated sites per bouton is increased by presynaptic PMCA knock down, with many neighboring sites being co-activated. False color coded images on the right show cumulative intensity distributions for 7 APs in control (A) and with PMCA knock down (B). **C** Quantification of total fluorescence normalized to bouton size reveals significantly increased responses in PMCA knock down (red circles) as compared to control (black triangles), and this is rescued by concomitant Ca_v1 knock-down.

4. Discussion

4.1 Two distinctly different voltage gated calcium channels localize to the presynaptic terminal of Drosophila larval crawling motoneurons

We confirm the localization of the Ca_v2 homolog Dmca1A to the active zone of presynaptic terminals, where it induces synaptic vesicle release upon action potential invasion, as previously been demonstrated (Gratz et al., 2019; Kawasaki et al., 2002; Kittel et al., 2006). Excitation secretion coupling of tightly coupled VGCCs, typically Ca_v2 channels, is one of the best described biological processes and is highly conserved across species (Dolphin and Lee, 2020). In addition, we reveal the presynaptic localization of another voltage gated calcium channel, the Ca_v1 homolog Dmca1D. We show its localization outside the active zone and a contribution to action potential induced calcium influx into the presynaptic terminal of about 50%, while having only a minor contribution to single AP evoked synaptic vesicle release, but significantly affecting short-term plasticity. We also show, that calcium influx through the Dmca1D channel has a significant contribution to synaptic vesicle endocytosis. The existence of Ca_v 1 and Ca_v 2 channels to presynaptic terminals could also be shown in other model systems. EM images from hippocampal neurons show the presynaptic localization of Ca_v 1 outside the active zone, but its function remains elusive (Tippens et al., 2008). Pharmacological experiments in vertebrate synapses indicate that presynaptic Ca_v1 channels do not contribute to synaptic vesicle release, but have functions in short-term plasticity (Subramanian and Morozov, 2011), long-term potentiation (Fourcaudot et al., 2009) and post-tetanic potentiation (Jensen and Mody, 2001). Additionally, data from the mouse NMJ provide anatomical and physiological (Pagani et al., 2004; Urbano and Uchitel, 1999) evidence of the presence of Ca_v1 and Ca_v2 channels, where synaptic vesicle release is mediated via the Ca_v2 channels, whereas Ca_v1 only has minor contribution to release.

This indicates that the colocalization of Ca_v1 and Ca_v2 channels to presynaptic terminals and division of labor between Ca_v2 for vesicle release, and Ca_v1 for the regulation and fine tuning of presynaptic plasticity, is a conserved mechanism across species and not a specialization of the *Drosophila* NMJ. In addition, we now provide a mechanism of how these calcium-depended processes are functionally separated in the minimal space of presynaptic terminals.

4.2 Dmca1D as a calcium source for the regulation of synaptic vesicle endocytosis

We show that Dmca1D knockdown increases synaptic depression upon prolonged stimulation. This provides indirect evidence for a contribution of Dmca1D to synaptic vesicle recycling. Direct optical measurements of synaptic vesicle endocytosis reveal a significant reduction of FM1-43 uptake into recycled vesicles upon Dmca1D knockdown, but no effect on dye unloading upon re-stimulation. This confirms the hypothesis that AP-triggered calcium influx through Dmca1D enhances SV endocytosis without contributing to SV release. Endocytosis regulation via activity dependent calcium influx has been debated for many years for vertebrate and invertebrate synapses (Leitz and Kavalali, 2015), in particular the calcium source for endocytosis regulation. For the *Drosophila* NMJ, different entry routes for synaptic vesicle release and recycling (Kuromi et al., 2004, 2010) and two different endocytotic modes, calcium dependent and independent (Koenig and Ikeda, 1996) are proposed. The vesicle associated calcium channel Flower is discussed to be the calcium source for the activity dependent regulation of vesicle endocytosis (Yao et al., 2009, 2017). To date, even though Flower is supposed to be conserved across all species (Yao et al., 2009), these findings could not be reproduced either in other species or by other *Drosophila* labs. We propose that the Dmca1D channel, localized outside the active zone where endocytosis takes place, is the calcium source for activity dependent regulation of synaptic vesicle endocytosis. Because endocytosis is reduced and not abolished upon Dmca1D knockdown, Dmca1D is not required for endocytosis to happen at all, but it has an augmenting effect. At small central synapses reacidification measurements and FM1-43 imaging support the idea, that calcium is used as an activity dependent switch between a fast and a slow endocytic mode (Zhu et al., 2009). We hypothesize that at the *Drosophila* NMJ Dmca1D provides the calcium signal to switch between endocytotic modes. Dmca1D is localized outside the active zone, where most endocytic processes occur. Its slow inactivation kinetics and big single channel conductance, typical for L-Type calcium channels, produce a big and long-lasting calcium inward current. Therefore, its location and biophysical properties make Dmca1D well suited to provide the high calcium concentrations over longer timescales needed for synaptic vesicle endocytosis. The Dmca1A channel on the other hand, which is localized in the active zone, displays fast activation and inactivation kinetics

and smaller single channel conductances, typical for a Ca_v2 channel, which are well suited to ensure tight coupling of AP invasion and neurotransmitter secretion.

The exact downstream mechanisms of the Dmca1D calcium signal still need to be investigated, but Ca_v1 dependent vesicle sorting in different vesicle pools has been shown in different studies. Ca_v1 channels are used to maintain synaptic transmission during high frequency firing at GABAergic synapses, and it has been speculated that Ca_v1 activation serves to move recycled vesicles directly into the readily releasable pool (Jensen and Mody, 2001). Pharmacological studies from the mouse NMJ provide indirect evidence for the hypothesis that Ca_v1 channels are necessary to recycle vesicles into a high probability release pool (Perissinotti et al., 2008), thus suggesting that endocytosis regulation via Ca_v1 channels may be a conserved mechanisms from invertebrates to vertebrates.

Together with Dmca1Ds functions in dendrites and the axon, where it functions to ensure high-frequency MN firing rates by boosting synaptic input and enabling fast action potential firing (Kadas et al., 2017), activity dependent regulation of endocytosis rates would be another synergistic contribution of Dmca1D to high frequency MN output. Because of its functions in all three neuronal compartments, Dmca1D increases the dynamic range in which a neuron can operate, which is further enlarged by its modulation via the biogenic amine tyramine (Schützler et al., 2019).

4.3 PMCA protects the active zone from external calcium sources

The plasma membrane bound calcium ATPase PMCA allows simultaneous calcium domains needed for separate exo- and endocytosis regulation in the limited space of presynaptic terminals. Most studies investigating the presynaptic effects of PMCA have focused on its function in maintaining overall calcium levels to prevent high cytosolic calcium concentrations, which can lead to cell death (Erhardt et al., 2019), or analyzed its function in calcium maintenance before and after activity (Lnenicka et al., 2006). Because PMCA is strongly enriched in the subsynaptic reticulum of the postsynapse, its precise localization within the presynaptic terminal remained difficult to uncover. By utilizing a postsynaptic knockdown of PMCA, we could show, that the PMCA is strategically localized outside the active zone and protects it from external calcium influx rather than protecting the cytosol from increased calcium concentrations through nanodomains. Subcellular localization of PMCA to fulfill specific, local functions was also shown in T-cells to steer calcium dependent processes in specific subcellular

calcium microdomains (Korthals et al., 2017; Quintana et al., 2011). Another subcellular function of PMCA pumps was found in dendritic spines of hippocampal neurons, where nonlinear calcium signaling orchestrated by PMCA is described to modulate the induction of synaptic plasticity (Scheuss et al., 2006). This shows, that the PMCA not only functions to maintain intracellular calcium concentrations at physiological levels but also enables subcellular calcium microdomains for specific local functions. PMCAs subcellular function at presynaptic terminals, uncovered in this thesis, expands the underlying concept of controlling release probability with soluble buffers and fixed buffers within the active zone (Delvendahl et al., 2015; Eggermann et al., 2013) by the idea of protecting the nanodomain from external, presynaptic calcium signals during activity by membrane anchored buffers with strategic localization outside active zones.

4.4 How does the interplay between Dmca1A, Dmca1D and PMCA extend the concept of synaptic strength and presynaptic plasticity?

Synaptic strength can be quantified based on the quantal theory of synaptic transmission (Katz, 1969; Rebola et al., 2019) by three parameters: number of release sites (N), the probability of action potential induced synaptic vesicle fusion (P_v) and the quantal size of the postsynaptic response (q). Especially PMCA and Dmca1D are two new variables affecting the probability of synaptic vesicle release. As we show that knockdown of Dmca1D leads to increased paired pulse facilitation, meaning that under normal conditions, P_v during the first stimulus is increased by the presence of Dmca1D. Knockdown of PMCA, on the other hand, leads to significantly increased transmitter release, therefore under normal conditions PMCA reduces P_v. If we now take into consideration, that PMCA and Dmca1D, the two factors that influence P_v are themselves subject to modulation; PMCA via pH (Lnenicka et al., 2006), acidic phospholipids, phosphorylation of serine, threonine and tyrosine at the C-Terminus, proteolytic dimerization of the C-Terminus and calcium (Strehler et al., 2007), while Dmca1D is modulated via Tyramine (Schützler et al., 2019), this results in metaplasticity of release probability. This is further potentiated by PMCAs ability to display a memory caused by slow unbinding kinetics of calmodulin at the C-Terminus, which vary between isoforms(Lopreiato et al., 2014; Strehler et al., 2007) and remaining in a preactivated state allowing fast responses to the next calcium stimulus (Caride et al., 2001). Additionally, structural diversity of PMCAs caused by alternative

splicing greatly change their properties in initial calcium response, inactivation rate and extrusion kinetics. For example, the vertebrate splice variants PMCA4a and PMCA4b, which only differ in the length of their C-Terminus, exhibit fundamentally different timescales in calcium response and inactivation rates. PMCA4a activates and inactivates very fast and is more efficient in handling transient calcium spikes. Whereas PMCA4b activates slow and inactivates very slow and is well suited to handle slow and tonic calcium changes (Strehler et al., 2007). Taken together, the structural and functional diversity of PMCA isoforms together with various possibilities of post-translational modulations, PMCA itself is a highly dynamic protein which has the potential to fundamentally increase the dynamic properties of the presynapse.

Another variable that influences P_v is the relative distance between synaptic vesicles and VGCCs. When VGCCs and vesicles are in close proximity, this so-called tight coupling results in a high P_v (0.3-0.8). Greater distances between VGCCs and vesicles result in weak coupling, and these synapses have low P_v values (~0.2) (Rebola et al., 2019). We can observe both cases at the *Drosophila* NMJ; the Dmca1A channel in the active zone is tightly coupled and the Dmca1D outside the active zone is loosely coupled. Taking in consideration that calcium channels can move to a certain degree inside the plasma membrane (Schneider et al., 2015) the relative distance of the channels to the vesicles change continuously. Given that the Dmca1A is inside the active zone and held in place by scaffolding proteins its ability to move is limited and should not change P_v in a drastic manner. Alternative splicing of vertebrate $Ca_v2.1$ C-Termini results in different protein length and effects the abundance of calcium channels within the active zone (Heck et al., 2019). This remains to be tested for Dmca1A, but if it also applies, it probably would have a more profound effect on vesicle coupling than movements of the channel within the active zone.

Investigating potential movements within the presynaptic membrane outside the active zone of both, PMCA and Dmca1D, and the resulting effects on vesicle coupling and synaptic strength could provide further insights into the understanding of presynaptic plasticity. Because presynaptic plasticity is more sensitive to loose coupled channels (Rebola et al., 2019), such as the Dmca1D, changes in Dmca1Ds distance to the active zone and changes in buffering-efficiency of its calcium signal by the PMCA have great potential in dynamically effecting P_v. But this hypothesis needs to be tested in further experiments along with possible interactions of PMCA and Dmca1D with scaffolding proteins outside the active zone.

Taken together, this thesis provides a new mechanism of how the weak coupled VGCC Dmca1D, localized outside the active zone of presynaptic terminals, provides calcium signals for: 1) activity dependent regulation of synaptic vesicle endocytosis and 2) presynaptic plasticity, without interfering with the calcium signal of the tight coupled VGCC Dmca1A inside the active zone. This is enabled by active buffering by the membrane bound calcium ATPase PMCA, to protect the active zone from external calcium signals. This mechanism has not been described before and increases the understanding of presynaptic calcium handling during activity. Additionally, the dynamic modulation of Dmca1D and PMCA takes the understanding of presynaptic plasticity to a metaplastic level.

5. References

Bagur, R., and Hajnóczky, G. (2017). Intracellular Ca 2+ Sensing: Its Role in Calcium Homeostasis and Signaling. Mol. Cell *66*, 780–788.

Berridge, M.J., Lipp, P., and Bootman, M.D. (2000). The versatility and universality of calcium signalling. Nat. Rev. Mol. Cell Biol. *1*, 11–21.

Brown, B.L., Walker, S.W., and Tomlinson, S. (1985). Calcium Calmodulin and Hormone Secretion. Clin. Endocrinol. (Oxf). *23*, 201–218.

Calì, T., Brini, M., and Carafoli, E. (2017). Regulation of Cell Calcium and Role of Plasma Membrane Calcium ATPases. Int. Rev. Cell Mol. Biol. *332*, 259–296.

Caride, A.J., Penheiter, A.R., Filoteo, A.G., Bajzer, Z., Enyedi, Á., and Penniston, J.T. (2001). The plasma membrane calcium pump displays memory of past calcium spikes: Differences between isoforms 2b and 4b. J. Biol. Chem. *276*, 39797–39804.

Catterall, W.A. (2011). Voltage-Gated Calcium Channels. Cold Spring Harb. Perspect. Biol. *3*, a003947–a003947.

Catterall, W.A., Striessnig, J., Snutch, T.P., and Perez-Reyes, E. (2003). International Union of Pharmacology. XL. Compendium of Voltage-Gated Ion Channels: Calcium Channels. Pharmacol. Rev. *55*, 579–581.

Caussinus, E., Kanca, O., and Affolter, M. (2012). Fluorescent fusion protein knockout mediated by anti-GFP nanobody. Nat. Struct. Mol. Biol. *19*, 117–121.

Chanaday, N.L., and Kavalali, E.T. (2020). Is Ca2+ Essential for Synaptic Vesicle Endocytosis? Trends Neurosci. *43*, 77–79.

Chen, T.W., Wardill, T.J., Sun, Y., Pulver, S.R., Renninger, S.L., Baohan, A., Schreiter, E.R., Kerr, R.A., Orger, M.B., Jayaraman, V., et al. (2013). Ultrasensitive fluorescent proteins for imaging neuronal activity. Nature *499*, 295–300.

Cousin, M.A., and Robinson, P.J. (2000). Ca2+ influx inhibits dynamin and arrests synaptic vesicle endocytosis at the active zone. J. Neurosci. *20*, 949–957.

Deligeorgiev, T., Vasilev, A., Kaloyanova, S., and Vaquero, J.J. (2010). Styryl dyes - synthesis and applications during the last 15 years. Color. Technol. *126*, 55–80.

Delvendahl, I., Jablonski, L., Baade, C., Matveev, V., Neher, E., and Hallermann, S. (2015). Reduced endogenous Ca2+ buffering speeds active zone Ca2+ signaling. Proc. Natl. Acad. Sci. U. S. A. *112*, E3075–E3084.

Dolmetsch, R.E., Pajvani, U., Fife, K., Spotts, J.M., and Greenberg, M.E. (2001). Signaling to the nucleus by an L-type calcium channel- calmodulin complex through the MAP kinase pathway. Science (80-.). *294*, 333–339.

Dolphin, A.C. (2016). Voltage-gated calcium channels and their auxiliary subunits: physiology and pathophysiology and pharmacology. J. Physiol. *1*, 1–22.

Dolphin, A.C. (2018). Voltage-gated calcium channels: Their discovery, function and importance as drug targets. Brain Neurosci. Adv. *2*, 1–8.

Dolphin, A.C., and Lee, A. (2020). Presynaptic calcium channels: specialized control of synaptic neurotransmitter release. Nat. Rev. Neurosci.

Eberl, D.F., Ren, D., Feng, G., Lorenz, L.J., Van Vactor, D., and Hall, L.M. (1998). Genetic and developmental characterization of Dmca1D, a calcium channel α1 subunit gene in Drosophila melanogaster. Genetics *148*, 1159–1169.

Eggermann, E., Bucurenciu, I., Goswami, S.P., and Jonas, P. (2013). Nanodomain coupling between Ca2+ channels and sensors of exocytosis at fast mammalian synapses. Nat Rev Neurosci *13*, 7–21.

Erhardt, B., Leal, M.C., Marcora, M.S., Frenkel, L., Bochicchio, P.A., Bodin, D.H., Silva, B.A., Farías, M.I., Ferrari, C.C., Allo, M.Á., et al. (2019). “Plasma Membrane Calcium Atpase downregulation in dopaminergic neurons alters cellular physiology and behavior in Drosophila melanogaster.” BioRxiv 714147.

Fatt, B.Y.P., and Katz, B. (1952). The Electrical Properties of Crustacean Muscle Fibres. J. Physiol. *120*, 171–204.

Fatt, P., and Ginsborg, B.L. (1958). The ionic requirements for the production of action potentials in crustacean muscle fibres. J. Physiol. *142*, 516–543.

Feng, Y., Ueda, A., and Wu, C.F. (2004). A modified minimal hemolymph-like solution, HL3.1, for physiological recordings at the neuromuscular junctions of normal and mutant Drosophila larvae. J. Neurogenet. *18*, 377–402.

Fisher, Y.E., Yang, H.H., Isaacman-Beck, J., Xie, M., Gohl, D.M., and Clandinin, T.R. (2017). FlpStop, a tool for conditional gene control in Drosophila. Elife *6*.

Flybase FlyBase Gene Report: Dmel\Ca-α1D.

Flybase FlyBase Gene Report: Dmel\PMCA.

Fourcaudot, E., Gambino, F., Casassus, G., Poulain, B., Humeau, Y., and Lüthi, A. (2009). L-type voltage-dependent Ca2+ channels mediate expression of presynaptic LTP in amygdala.

Nat. Neurosci. *12*, 1093–1095.

Gan, Q., and Watanabe, S. (2018). Synaptic Vesicle Endocytosis in Different Model Systems. Front. Cell. Neurosci. *12*, 171.

Gandhi, S.P., and Stevens, C.F. (2003). Three modes of synaptic vesicular recycling revealed by single-vesicle imaging. Nature *423*, 607–613.

Gaudet, P., Livstone, M.S., Lewis, S.E., and Thomas, P.D. (2011). Phylogenetic-based propagation of functional annotations within the Gene Ontology consortium. Brief. Bioinform. *12*, 449–462.

Genç, Ö., and Davis, G.W. (2019). Target-wide Induction and Synapse Type-Specific Robustness of Presynaptic Homeostasis. Curr. Biol. *29*, 3863-3873.e2.

Genç, Ö., Dickman, D.K., Ma, W., Tong, A., Fetter, R.D., and Davis, G.W. (2017). MCTP is an ER-resident calcium sensor that stabilizes synaptic transmission and homeostatic plasticity. Elife *6*, 1–23.

Gerber, S.H., and Sudhof, T.C. (2002). Section 1: Insulin Release: Some Molecular Requisites Molecular Determinants of Regulated Exocytosis. Diabetes *51*, 3–11.

Gerber, S.H., Garcia, J., Rizo, J., and Südhof, T.C. (2001). An unusual C2-domain in the active-zone protein piccolo: Implications for Ca2+ regulation of neurotransmitter release. EMBO J. *20*, 1605–1619.

Granseth, B., Odermatt, B., Royle, S.J., and Lagnado, L. (2009). Comment on “the dynamic control of kiss-and-run and vesicular reuse probed with single nanoparticles.” Science (80-.). *325*.

Gratz, S.J., Goel, P., Bruckner, J.J., Hernandez, R.X., Khateeb, K., Macleod, G.T., Dickman, D., and O’Connor-Giles, K.M. (2019). Endogenous tagging reveals differential regulation of Ca2+ channels at single active zones during presynaptic homeostatic potentiation and depression. J. Neurosci. *39*, 2416–2429.

Green, E.W., Fedele, G., Giorgini, F., and Kyriacou, C.P. (2014). A Drosophila RNAi collection is subject to dominant phenotypic effects. Nat. Methods *11*, 222–223.

Hara, Y., Koganezawa, M., and Yamamoto, D. (2015). The Dmca1D channel mediates Ca2+ inward currents in Drosophila embryonic muscles. J. Neurogenet. *29*, 117–123.

Hardingham, G.E., Cruzalegui, F.H., Chawla, S., and Bading, H. (1998). Mechanisms controlling gene expression by nuclear calcium signals. Cell Calcium *23*, 131–134.

Haucke, V., Neher, E., and Sigrist, S.J. (2011). Protein scaffolds in the coupling of synaptic

exocytosis and endocytosis. Nat. Rev. Neurosci. *12*, 127–138.

Heck, J., Parutto, P., Ciuraszkiewicz, A., Bikbaev, A., Freund, R., Mitlöhner, J., Andres-Alonso, M., Fejtova, A., Holcman, D., and Heine, M. (2019). Transient Confinement of CaV2.1 Ca2+-Channel Splice Variants Shapes Synaptic Short-Term Plasticity. Neuron *103*, 66–79.

Heckman, C.J., Lee, R.H., and Brownstone, R.M. (2003). Hyperexcitable dendrites in motoneurons and their neuromodulatory control during motor behavior. Trends Neurosci. *26*, 688–695.

Heerssen, H., Fetter, R.D., and Davis, G.W. (2008). Clathrin Dependence of Synaptic-Vesicle Formation at the Drosophila Neuromuscular Junction. Curr. Biol. *18*, 401–409.

Heilbrunn, L. V., and Wiercinski, F.J. (1947). The action of various cations on muscle protoplasm. J. Cell. Comp. Physiol. *29*, 15–32.

Heinrich, L., and Ryglewski, S. (2019). Different α 2 δ Accessory Subunits Regulate Distinctly Different Aspects of Calcium Channel Function in the Same Drosophila Neurons. BioRxiv.

Hille, B. (2001). Ion channels of excitable membranes (Sinauer).

Holt, M., Cooke, A., Wu, M.M., and Lagnado, L. (2003). Bulk membrane retrieval in the synaptic terminal of retinal bipolar cells. J. Neurosci. *23*, 1329–1339.

Hosoi, N., Holt, M., and Sakaba, T. (2009). Calcium Dependence of Exo- and Endocytotic Coupling at a Glutamatergic Synapse. Neuron *63*, 216–229.

Hurlbut, W.P., and Ceccarelli, B. (1974). Transmiter Release and Recycling of Synaptic Vesicle Membrane at the Neuromuscular Junction. Adv Cytopharmacol *2*, 141–154.

Hutchinson, T.E., Zhong, W., Chebolu, S., Wilson, S.M., and Darmani, N.A. (2015). L-type calcium channels contribute to 5-HT3-receptor-evoked CaMKIIα and ERK activation and induction of emesis in the least shrew (Cryptotis parva). Eur. J. Pharmacol. *755*, 110–118.

Islam, M.S. (2020). Calcium signaling (CRC Press).

Jacus, M.O., Uebele, V.N., Renger, J.J., and Todorovic, S.M. (2012). Presynaptic CaV3.2 channels regulate excitatory neurotransmission in nociceptive dorsal horn neurons. J. Neurosci. *32*, 9374–9382.

Jan, L.Y., and Jan, Y.N. (1976). Properties of the larval neuromuscular junction in Drosophila melanogaster. J. Physiol. *262*, 189–214.

Jensen, K., and Mody, I. (2001). L-type Ca2+ channel-mediated short-term plasticity of GABAergic synapses. Nat. Neurosci. *4*, 975–976.

Johnson, B.R., Hauptman, S.A., and Bonow, R.H. (2007). Construction of a Simple Suction Electrode for Extracellular Recording and Stimulation. J. Undergrad. Neurosci. Educ. *6*, A21.

Kadas, D., Ryglewski, S., and Duch, C. (2015). Transient BK outward current enhances motoneurone firing rates during Drosophila larval locomotion. J. Physiol. *22*, 4871–4888.

Kadas, D., Klein, A., Krick, N., Worrell, J.W., Ryglewski, S., and Duch, C. (2017). Dendritic and axonal L-type calcium channels cooperate to enhance motoneuron firing output during Drosophila larval locomotion. J. Neurosci. *37*, 10971–10982.

Kanamori, T., Kanai, M.I., Dairyo, Y., Yasunaga, K.I., Morikawa, R.K., and Emoto, K. (2013). Compartmentalized calcium transients trigger dendrite pruning in Drosophila sensory neurons. Science (80-.). *340*, 1475–1478.

Katz, B. (1969). The release of neural transmitter substances. Liverpool Univ. Press 5–39.

Katz, B., and Miledi, R. (1966). A Study of Synaptic Transmission in the Absence of Nerve Impulses. J. Physiol. *192*, 407–436.

Kawasaki, F., Collins, S.C., and Ordway, R.W. (2002). Synaptic calcium-channel function in Drosophila: analysis and transformation rescue of temperature-sensitive paralytic and lethal mutations of cacophony. J. Neurosci. *22*, 5856–5864.

Kern, J. V., Zhang, Y. V., Kramer, S., Brenman, J.E., and Rasse, T.M. (2013). The Kinesin-3, Unc-104 Regulates Dendrite Morphogenesis and Synaptic Development in Drosophila. Genetics *195*, 59–72.

Khvotchev, M., Lonart, G., and Südhof, T.C. (2000). Role of calcium in neurotransmitter release evoked by α-latrotoxin or hypertonic sucrose. Neuroscience *101*, 793–802.

King, G.F. (2007). Modulation of insect Cav channels by peptidic spider toxins. Toxicon *49*, 513–530.

Kiragasi, B., Wondolowski, J., Li, Y., and Dickman, D.K. (2017). A Presynaptic Glutamate Receptor Subunit Confers Robustness to Neurotransmission and Homeostatic Potentiation. Cell Rep. *19*, 2694–2706.

Kittel, R.J., Wichmann, C., Rasse, T.M., Fouquet, W., Schmidt, M., Schmid, A., Wagh, D. a, Pawlu, C., Kellner, R.R., Willig, K.I., et al. (2006). Bruchpilot promotes Active zone assembly, Ca2+ channel clustering and vesicle release. Science (80-.). *312*, 1051–1054.

Klein, A. (2016). Presynaptic function of the voltage-gated calcium channel DmCa1D in Drosophila larval motoneurons. Johannes Gutenberg-University Mainz.

Klein, M., Shapiro, E., and Kandel, E.R. (1980). Synaptic plasticity and the modulation of the

Ca2+ current. J. Exp. Biol. *89*, 117–157.

Klingauf, J., Kavalali, E.T., and Tsien, R.W. (1998). Kinetics and regulation of fast endocytosis at hippocampal synapses. Nature *394*, 581–585.

Koenig, J.H., and Ikeda, K. (1996). Synaptic vesicles have two distinct recycling pathways. J. Cell Biol. *135*, 797–808.

Koh, Y.H., Popova, E., Thomas, U., Griffith, L.C., and Budnik, V. (1999). Regulation of DLG Localization at Synapses by CaMKII-Dependent Phosphorylation. Cell *98*, 353–363.

Kononenko, N.L., and Haucke, V. (2015). Molecular mechanisms of presynaptic membrane retrieval and synaptic vesicle reformation. Neuron *85*, 484–496.

Kononenko, N.L., Puchkov, D., Classen, G.A., Walter, A.M., Pechstein, A., Sawade, L., Kaempf, N., Trimbuch, T., Lorenz, D., Rosenmund, C., et al. (2014). Clathrin/AP-2 mediate synaptic vesicle reformation from endosome-like vacuoles but are not essential for membrane retrieval at central synapses. Neuron *82*, 981–988.

Korthals, M., Langnaese, K., Smalla, K.H., Kähne, T., Herrera-Molina, R., Handschuh, J., Lehmann, A.C., Mamula, D., Naumann, M., Seidenbecher, C., et al. (2017). A complex of Neuroplastin and Plasma Membrane Ca2+ ATPase controls T cell activation. Sci. Rep. *7*, 1–13.

Krebs, J. (2017). The Plasma Membrane Calcium Pump (PMCA): Regulation of Cytosolic Ca2+, Genetic Diversities and Its Role in Sub-plasma Membrane Microdomains. In Advances in Experimental Medicine and Biology, pp. 3–21.

Kuromi, H., Honda, A., and Kidokoro, Y. (2004). Ca2+ Influx through Distinct Routes Controls Exocytosis and Endocytosis at Drosophila Presynaptic Terminals. Neuron *41*, 101–111.

Kuromi, H., Ueno, K., and Kidokoro, Y. (2010). Two types of Ca2+ channel linked to two endocytic pathways coordinately maintain synaptic transmission at the Drosophila synapse. Eur. J. Neurosci. *32*, 335–346.

Laine, R.F., Tosheva, K.L., Gustafsson, N., Gray, R.D.M., Almada, P., Albrecht, D., Risa, G.T., Hurtig, F., Lindås, A.C., Baum, B., et al. (2019). NanoJ: A high-performance open-source super-resolution microscopy toolbox. J. Phys. D. Appl. Phys. *52*.

Lee, J., and Wu, C.F. (2010). Orchestration of stepwise synaptic growth by K+ and Ca 2+ channels in Drosophila. J. Neurosci. *30*, 15821–15833.

Lee, T., and Luo, L. (2001). Mosaic analysis with a repressible cell marker (MARCM) for Drosophila neural development. Trends Neurosci. *24*, 251–254.

Lee, J., Ueda, A., and Wu, C.F. (2008). Pre- and post-synaptic mechanisms of synaptic strength homeostasis revealed by slowpoke and shaker K+ channel mutations in Drosophila. Neuroscience *154*, 1283–1296.

Lee, J., Ueda, A., and Wu, C.F. (2014). Distinct roles of Drosophila cacophony and Dmca1D Ca2+ channels in synaptic homeostasis: Genetic interactions with slowpoke Ca2+-activated BK channels in presynaptic excitability and postsynaptic response. Dev. Neurobiol. *74*, 1–15.

Leitz, J., and Kavalali, E.T. (2015). Ca2+ Dependence of Synaptic Vesicle Endocytosis. Neurosci. *22*, 464–476.

Littleton, J.T., and Ganetzky, B. (2000). Ion channels and synaptic organization: Analysis of the Drosophila genome. Neuron *26*, 35–43.

Llinás, R., Sugimori, M., and Silver, R.B. (1992). Microdomains of high calcium concentration in a presynaptic terminal. Science (80-.). *256*, 677–679.

Lnenicka, G.A., Grizzaffi, J., Lee, B., and Rumpal, N. (2006). Ca2+ dynamics along identified synaptic terminals in Drosophila larvae. J. Neurosci. *26*, 12283–12293.

Lopreiato, R., Giacomello, M., and Carafoli, E. (2014). The plasma membrane calcium pump: New ways to look at an old enzyme. J. Biol. Chem. *289*, 10261–10268.

Lowe, N., Rees, J.S., Roote, J., Ryder, E., Armean, I.M., Johnson, G., Drummond, E., Spriggs, H., Drummond, J., Magbanua, J.P., et al. (2014). Analysis of the expression patterns, Subcellular localisations and interaction partners of drosophila proteins using a pigp protein trap library. Dev. *141*, 3994–4005.

Luo, F., and Südhof, T.C. (2017). Synaptotagmin-7-Mediated Asynchronous Release Boosts High-Fidelity Synchronous Transmission at a Central Synapse. Neuron *94*, 826-839.e3.

MacPherson, M.R., Pollock, V.P., Broderick, K.E., Kean, L., O'Connell, F.C., Dow, J.A.T., and Davies, S.A. (2001). Model organisms: New insights into ion channel and transporter function. L-type calcium channels regulate epithelial fluid transport in Drosophila melanogaster. Am. J. Physiol. - Cell Physiol. *280*, 394–407.

Mahr, A., and Aberle, H. (2006). The expression pattern of the Drosophila vesicular glutamate transporter: A marker protein for motoneurons and glutamatergic centers in the brain. Gene Expr. Patterns *6*, 299–309.

Maritzen, T., and Haucke, V. (2017). Coupling of exocytosis and endocytosis at the presynaptic active zone. Neurosci. Res. *127*, 45–52.

Moosmang, S., Haider, N., Klugbauer, N., Adelsberger, H., Langwieser, N., Müller, J., Stiess,

M., Marais, E., Schulla, V., Lacinova, L., et al. (2005). Journal of Neuroscience. J. Neurosci. *20*, 3714–3724.

Murthy, V.N., and Stevens, C.F. (1998). Synaptic vesicles retain their identity through the endocytic cycle. Nature *392*, 497–501.

Nakai, J., Ohkura, M., and Imoto, K. (2001). A high signal-to-noise Ca(2+) probe composed of a single green fluorescent protein. Nat. Biotechnol. *19*, 137–141.

Nanou, E., and Catterall, W.A. (2018). Calcium Channels, Synaptic Plasticity, and Neuropsychiatric Disease. Neuron *98*, 466–481.

Ni, J.Q., Markstein, M., Binari, R., Pfeiffer, B., Liu, L.P., Villalta, C., Booker, M., Perkins, L., and Perrimon, N. (2008). Vector and parameters for targeted transgenic RNA interference in Drosophila melanogaster. Nat. Methods *5*, 49–51.

Ni, J.Q., Liu, L.P., Binari, R., Hardy, R., Shim, H.S., Cavallaro, A., Booker, M., Pfeiffer, B.D., Markstein, M., Wang, H., et al. (2009). A drosophila resource of transgenic RNAi lines for neurogenetics. Genetics *182*, 1089–1100.

Ono, Y., Mori, Y., Egashira, Y., Sumiyama, K., and Takamori, S. (2019). Expression of plasma membrane calcium ATPases confers Ca2+/H+ exchange in rodent synaptic vesicles. Sci. Rep. *9*, 4289.

Orlando, M., Schmitz, D., Rosenmund, C., and Herman, M.A. (2019). Calcium-Independent Exo-endocytosis Coupling at Small Central Synapses. Cell Rep. *29*, 3767-3774.e3.

Pagani, R., Song, M., Mcenery, M., Qin, N., Tsien, R.W., Toro, L., Stefani, E., and Uchitel, O.D. (2004). Differential expression of α1 and β subunits of voltage dependent Ca2+ channel at the neuromuscular junction of normal and P/Q Ca2+ channel knockout mouse. Neuroscience *123*, 75–85.

Pedersen, B.P., Buch-Pedersen, M.J., Preben Morth, J., Palmgren, M.G., and Nissen, P. (2007). Crystal structure of the plasma membrane proton pump. Nature *450*, 1111–1114.

Perissinotti, P.P., Tropper, B.G., and Uchitel, O.D. (2008). L-type calcium channels are involved in fast endocytosis at the mouse neuromuscular junction. Eur. J. Neurosci. *27*, 1333–1344.

Petzoldt, A.G., Lützkendorf, J., and Sigrist, S.J. (2016). Mechanisms controlling assembly and plasticity of presynaptic active zone scaffolds. Curr. Opin. Neurobiol. *39*, 69–76.

Qu, L., Akbergenova, Y., Hu, Y., and Schikorski, T. (2009). Synapse-to-synapse variation in mean synaptic vesicle size and its relationship with synaptic morphology and function. J.

Comp. Neurol. *514*, 343–352.

Quintana, A., Pasche, M., Junker, C., Al-Ansary, D., Rieger, H., Kummerow, C., Nuñez, L., Villalobos, C., Meraner, P., Becherer, U., et al. (2011). Calcium microdomains at the immunological synapse: how ORAI channels, mitochondria and calcium pumps generate local calcium signals for efficient T-cell activation. EMBO J. *30*, 3895–3912.

Ramírez-Latorre, J.A. (2012). Functional Upregulation of Ca2+ -Activated K+ Channels in the Development of Substantia Nigra Dopamine Neurons. PLoS One *7*.

Rebola, N., Reva, M., Kirizs, T., Szoboszlay, M., Lőrincz, A., Moneron, G., Nusser, Z., and DiGregorio, D.A. (2019). Distinct Nanoscale Calcium Channel and Synaptic Vesicle Topographies Contribute to the Diversity of Synaptic Function. Neuron *104*, 693-710.e9.

Ren, D., Xu, H., Eberl, D.F., Chopra, M., and Hall, L.M. (1998). A mutation affecting dihydropyridine-sensitive current levels and activation kinetics in Drosophila muscle and mammalian heart calcium channels. J. Neurosci. *18*, 2335–2341.

Rieckhof, G.E., Yoshihara, M., Guan, Z., and Littleton, J.T. (2003). Presynaptic N-type Calcium Channels Regulate Synaptic Growth. J. Biol. Chem. *278*, 41099–41108.

Ringer, S. (1883). A Further Contribution Regarding the Inlfuence of the Different Constituents of the Blood on the Contraction of the Heart. J. Physiol. *4*, 29-42.3.

Ryglewski, S., Lance, K., Levine, R.B., and Duch, C. (2012). Ca(v)2 channels mediate low and high voltage-activated calcium currents in Drosophila motoneurons. J. Physiol. *590*, 809–825.

Sato, K., Ernstrom, G.G., Watanabe, S., Weimer, R.M., Chen, C.-H., Sato, M., Siddiqui, A., Jorgensen, E.M., and Grant, B.D. (2009). Differential requirements for clathrin in receptor-mediated endocytosis and maintenance of synaptic vesicle pools. Proc. Natl. Acad. Sci. *106*, 1139–1144.

Scheuss, V., Yasuda, R., Sobczyk, A., and Svoboda, K. (2006). Nonlinear [Ca2+] Signaling in Dendrites and Spines Caused by Activity-Dependent Depression of Ca2+ Extrusion. J. Neurosci. *26*, 8183–8194.

Schmidt, N., Kollewe, A., Constantin, C.E., Henrich, S., Ritzau-Jost, A., Bildl, W., Saalbach, A., Hallermann, S., Kulik, A., Fakler, B., et al. (2017). Neuroplastin and Basigin Are Essential Auxiliary Subunits of Plasma Membrane Ca2+-ATPases and Key Regulators of Ca2+ Clearance. Neuron *96*, 827-838.e9.

Schneggenburger, R., and Neher, E. (2005). Presynaptic calcium and control of vesicle fusion. Curr. Opin. Neurobiol. *15*, 266–274.

Schneider, R., Hosy, E., Kohl, J., Klueva, J., Choquet, D., Thomas, U., Voigt, A., and Heine, M. (2015). Mobility of Calcium Channels in the Presynaptic Membrane. Neuron *86*, 672–680.

Schützler, N., Girwert, C., Hügli, I., Mohana, G., Roignant, J.Y., Ryglewski, S., and Duch, C. (2019). Tyramine action on motoneuron excitability and adaptable tyramine/octopamine ratios adjust Drosophila locomotion to nutritional state. Proc. Natl. Acad. Sci. U. S. A. *116*, 3805–3810.

Sclip, A., Acuna, C., Luo, F., and Südhof, T.C. (2018). RIM -binding proteins recruit BK-channels to presynaptic release sites adjacent to voltage-gated Ca 2+ -channels . EMBO J. *37*, 1–14.

Simms, B.A., and Zamponi, G.W. (2014). Neuronal voltage-gated calcium channels: Structure, function, and dysfunction. Neuron *82*, 24–45.

Soykan, T., Maritzen, T., and Haucke, V. (2016). Modes and mechanisms of synaptic vesicle recycling. Curr. Opin. Neurobiol. *39*, 17–23.

Soykan, T., Kaempf, N., Sakaba, T., Vollweiter, D., Goerdeler, F., Puchkov, D., Kononenko, N.L., and Haucke, V. (2017). Synaptic Vesicle Endocytosis Occurs on Multiple Timescales and Is Mediated by Formin-Dependent Actin Assembly. Neuron *93*, 854-866.e4.

Stevens, C.F., and Williams, J.H. (2000). “Kiss and run” exocytosis at hippocampal synapses. Proc. Natl. Acad. Sci. U. S. A. *97*, 12828–12833.

Stewart, B.A., Atwood, H.L., Renger, J.J., Wang, J., and Wu, C.F. (1994). Improved stability of Drosophila larval neuromuscular preparations in haemolymph-like physiological solutions. J. Comp. Physiol. A *175*, 179–191.

Strehler, E.E., Filoteo, A.G., Penniston, J.T., and Caride, A.J. (2007). Plasma-membrane Ca2+ pumps: Structural diversity as the basis for functional versatility. In Biochemical Society Transactions, (Biochem Soc Trans), pp. 919–922.

Subramanian, J., and Morozov, A. (2011). Erk1/2 Inhibit Synaptic Vesicle Exocytosis through L-Type Calcium Channels. J. Neurosci. *31*, 4755–4764.

Südhof, T.C. (2004). The Synaptic Vesicle Cycle. Annu. Rev. Neurosci. *27*, 509–547.

Sugita, S., and Südhof, T.C. (2000). Specificity of Ca2+-dependent protein interactions mediated by the C2A domains of synaptotagmins. Biochemistry *39*, 2940–2949.

Tang, C., Presser, F., and Morad, M. (1988). Amiloride selectively blocks the low threshold (T) calcium channel. Science (80-.). *240*, 213–215.

Tedford, H.W., Maggio, F., Reenan, R.A., and King, G. (2007). A model genetic system for

testing the in vivo function of peptide toxins. Peptides *28*, 51–56.

Thomas, P., Lee, A.K., Wong, J.G., and Almers, W. (1994). A triggered mechanism retrieves membrane in seconds after Ca2+- stimulated exocytosis in single pituitary cells. J. Cell Biol. *124*, 667–675.

Tippens, A.L., Pare, J.-F., Langwieser, N., Moosmang, S., Milner, T.A., Smith, Y., and Lee, A. (2008). Ultrastructural evidence for pre- and postsynaptic localization of Cav1.2 L-type Ca2+ channels in the rat hippocampus. J. Comp. Neurol. *506*, 569–583.

Urbano, F.J., and Uchitel, O.D. (1999). L-Type calcium channels unmasked by cell-permeant Ca 2+ buffer at mouse motor nerve terminals. Eur. J. Physiol. *437*, 523–528.

Verstreken, P., Ohyama, T., and Bellen, H.J. (2008). FM 1-43 labeling of synaptic vesicle pools at the drosophila neuromuscular junction. Methods Mol. Biol. *440*, 349–369.

Voets, T., Moser, T., Lund, P.E., Chow, R.H., Geppert, M., Südhof, T.C., and Neher, E. (2001). Intracellular calcium dependence of large dense-core vesicle exocytosis in the absence of synaptotagmin I. Proc. Natl. Acad. Sci. U. S. A. *98*, 11680–11685.

Wagh, D.A., Rasse, T.M., Asan, E., Hofbauer, A., Schwenkert, I., Dürrbeck, H., Buchner, S., Dabauvalle, M.-C., Schmidt, M., Qin, G., et al. (2006). Bruchpilot, a Protein with Homology to ELKS/CAST, Is Required for Structural Integrity and Function of Synaptic Active Zones in Drosophila. Neuron *49*, 833–844.

Wang, H., Zhang, C., and Xiao, H. (2019). Mechanism of membrane fusion: protein-protein interaction and beyond. Int. J. Physiol. Pathophysiol. Pharmacol. *11*, 250–257.

Watanabe, S., and Boucrot, E. (2017). Fast and ultrafast endocytosis. Curr. Opin. Cell Biol. *47*, 64–71.

Watanabe, S., Liu, Q., Davis, M.W., Hollopeter, G., Thomas, N., Jorgensen, N.B., and Jorgensen, E.M. (2013a). Ultrafast endocytosis at Caenorhabditis elegans neuromuscular junctions. Elife *2013*.

Watanabe, S., Rost, B.R., Camacho-Pérez, M., Davis, M.W., Söhl-Kielczynski, B., Rosenmund, C., and Jorgensen, E.M. (2013b). Ultrafast endocytosis at mouse hippocampal synapses. Nature *504*, 242–247.

Watanabe, S., Trimbuch, T., Camacho-Pérez, M., Rost, B.R., Brokowski, B., Söhl-Kielczynski, B., Felies, A., Davis, M.W., Rosenmund, C., and Jorgensen, E.M. (2014). Clathrin regenerates synaptic vesicles from endosomes. Nature *515*, 228–233.

Wienisch, M., and Klingauf, J. (2006). Vesicular proteins exocytosed and subsequently

retrieved by compensatory endocytosis are nonidentical. Nat. Neurosci. *9*, 1019–1027.

Worrell, J.W., and Levine, R.B. (2008). Characterization of voltage-dependent Ca2+ currents in identified drosophila motoneurons in situ. J. Neurophysiol. *100*, 868–878.

Wu, J., Yan, Z., Li, Z., Qian, X., Lu, S., Dong, M., Zhou, Q., and Yan, N. (2016). Structure of the voltage-gated calcium channel Cav1.1 at 3.6 Å resolution. Nature *537*, 191–196.

Wu, X.-S., Zhang, Z., Zhao, W.-D., Wang, D., Luo, F., and Wu, L.-G. (2014). Calcineurin is universally involved in vesicle endocytosis at neuronal and non-neuronal secretory cells. Cell Rep. *7*, 982–988.

Xu, J., McNeil, B., Wu, W., Nees, D., Bai, L., and Wu, L.G. (2008). GTP-independent rapid and slow endocytosis at a central synapse. Nat. Neurosci. *11*, 45–53.

Yamashita, T. (2012). Ca 2+-dependent regulation of synaptic vesicle endocytosis. Neurosci. Res. *73*, 1–7.

Yao, C.K., Lin, Y.Q., Ly, C. V., Ohyama, T., Haueter, C.M., Moiseenkova-Bell, V.Y., Wensel, T.G., and Bellen, H.J. (2009). A Synaptic Vesicle-Associated Ca2+ Channel Promotes Endocytosis and Couples Exocytosis to Endocytosis. Cell *138*, 947–960.

Yao, C.K., Liu, Y.T., Lee, I.C., Wang, Y.T., and Wu, P.Y. (2017). A Ca2+channel differentially regulates Clathrin-mediated and activity-dependent bulk endocytosis. PLoS Biol. *15*.

Zamponi, G.W., Striessnig, J., Koschak, A., and Dolphin, A.C. (2015). The physiology, pathology, and pharmacology of voltage-gated calcium channels and their future therapeutic potential. Pharmacol. Rev. *67*, 821–870.

Zhang, J.Z., Davletov, B.A., Südhof, T.C., and Anderson, R.G.W. (1994). Synaptotagmin I is a high affinity receptor for clathrin AP-2: Implications for membrane recycling. Cell *78*, 751–760.

Zhang, Q., Li, Y., and Tsien, R.W. (2009). The Dynamic Control of Kiss-And-Run and Vesicular Reuse Probed with Single Nanoparticles. Science (80-.). *323*, 1448–1453.

Zhao, Y., Huang, G., Wu, Q., Wu, K., Li, R., Lei, J., Pan, X., and Yan, N. (2019). Cryo-EM structures of apo and antagonist-bound human Cav3.1. Nature *576*, 492–497.

Zheng, W., Feng, G., Ren, D., Eberl, D.F., Hannen, F., Dubald, M., and Hall, L.M. (1995). Cloning and characterization of a calcium channel α1 subunit from Drosophila melanogaster with similarity to the rat brain type D isoform. J. Neurosci. *15*, 1132–1143.

Zhu, Y., Xu, J., and Heinemann, S.F. (2009). Two Pathways of Synaptic Vesicle Retrieval Revealed by Single-Vesicle Imaging. Neuron *61*, 397–411.